Search for $\Upsilon(1S,2S) \to Z_c^+ Z_c^{(\prime)-}$ and $e^+e^- \to Z_c^+ Z_c^{(\prime)-}$ at $\sqrt{s} = 10.52, 10.58,$ and 10.867 GeV

S. Jia,[2] C. P. Shen,[2] C. Z. Yuan,[26] I. Adachi,[18,14] H. Aihara,[86] S. Al Said,[79,37] D. M. Asner,[3] V. Aulchenko,[4,67] T. Aushev,[55] R. Ayad,[79] V. Babu,[80] I. Badhrees,[79,36] V. Bansal,[69] P. Behera,[24] C. Beleño,[13] B. Bhuyan,[22] T. Bilka,[5] J. Biswal,[32] A. Bozek,[63] M. Bračko,[49,32] D. Červenkov,[5] V. Chekelian,[50] A. Chen,[60] B. G. Cheon,[16] K. Chilikin,[44] K. Cho,[38] S.-K. Choi,[15] Y. Choi,[78] S. Choudhury,[23] D. Cinabro,[90] S. Cunliffe,[7] N. Dash,[21] S. Di Carlo,[42] Z. Doležal,[5] S. Eidelman,[4,67] J. E. Fast,[69] T. Ferber,[7] B. G. Fulsom,[69] R. Garg,[70] V. Gaur,[89] N. Gabyshev,[4,67] A. Garmash,[4,67] M. Gelb,[34] A. Giri,[23] P. Goldenzweig,[34] E. Guido,[30] J. Haba,[18,14] T. Hara,[18,14] K. Hayasaka,[65] H. Hayashii,[59] M. T. Hedges,[17] S. Hirose,[56] W.-S. Hou,[62] T. Iijima,[57,56] K. Inami,[56] G. Inguglia,[7] A. Ishikawa,[84] R. Itoh,[18,14] M. Iwasaki,[68] W. W. Jacobs,[25] I. Jaegle,[9] H. B. Jeon,[41] Y. Jin,[86] T. Julius,[51] G. Karyan,[7] T. Kawasaki,[65] C. Kiesling,[50] D. Y. Kim,[76] H. J. Kim,[41] J. B. Kim,[39] K. T. Kim,[39] S. H. Kim,[16] K. Kinoshita,[6] P. Kodyš,[5] S. Korpar,[49,32] D. Kotchetkov,[17] P. Križan,[45,32] R. Kroeger,[52] P. Krokovny,[4,67] T. Kuhr,[46] R. Kulasiri,[35] T. Kumita,[88] Y.-J. Kwon,[92] J. S. Lange,[11] I. S. Lee,[16] S. C. Lee,[41] L. K. Li,[26] Y. Li,[89] Y. B. Li,[71] L. Li Gioi,[50] J. Libby,[24] D. Liventsev,[89,18] M. Lubej,[32] T. Luo,[10] J. MacNaughton,[18] M. Masuda,[85] T. Matsuda,[53] M. Merola,[29,58] K. Miyabayashi,[59] H. Miyata,[65] R. Mizuk,[44,54,55] H. K. Moon,[39] R. Mussa,[30] E. Nakano,[68] M. Nakao,[18,14] T. Nanut,[32] K. J. Nath,[22] Z. Natkaniec,[63] M. Nayak,[90,18] M. Niiyama,[40] S. Nishida,[18,14] S. Ogawa,[83] S. Okuno,[33] H. Ono,[64,65] P. Pakhlov,[44,54] G. Pakhlova,[44,55] B. Pal,[6] S. Pardi,[29] H. Park,[41] S. Paul,[82] T. K. Pedlar,[47] R. Pestotnik,[32] L. E. Piilonen,[89] V. Popov,[44,55] M. Ritter,[46] A. Rostomyan,[7] G. Russo,[29] Y. Sakai,[18,14] M. Salehi,[48,46] S. Sandilya,[6] L. Santelj,[18] T. Sanuki,[84] V. Savinov,[72] O. Schneider,[43] G. Schnell,[1,20] C. Schwanda,[27] Y. Seino,[65] K. Senyo,[91] M. E. Sevior,[51] V. Shebalin,[4,67] T.-A. Shibata,[87] J.-G. Shiu,[62] B. Shwartz,[4,67] F. Simon,[50,81] A. Sokolov,[28] E. Solovieva,[44,55] S. Stanič,[66] M. Starič,[32] J. F. Strube,[69] M. Sumihama,[12] T. Sumiyoshi,[88] M. Takizawa,[75,19,73] U. Tamponi,[30] K. Tanida,[31] F. Tenchini,[51] K. Trabelsi,[18,14] M. Uchida,[87] T. Uglov,[44,55] S. Uno,[18,14] P. Urquijo,[51] Y. Usov,[4,67] C. Van Hulse,[1] G. Varner,[17] A. Vinokurova,[4,67] V. Vorobyev,[4,67] A. Vossen,[8] B. Wang,[6] C. H. Wang,[61] M.-Z. Wang,[62] P. Wang,[26] X. L. Wang,[10] M. Watanabe,[65] E. Widmann,[77] E. Won,[39] H. Ye,[7] S. Zakharov,[44,55] Z. P. Zhang,[74] V. Zhilich,[4,67] V. Zhukova,[44,54] V. Zhulanov,[4,67] and A. Zupanc[45,32]

(Belle Collaboration)

[1]*University of the Basque Country UPV/EHU, 48080 Bilbao*
[2]*Beihang University, Beijing 100191*
[3]*Brookhaven National Laboratory, Upton, New York 11973*
[4]*Budker Institute of Nuclear Physics SB RAS, Novosibirsk 630090*
[5]*Faculty of Mathematics and Physics, Charles University, 121 16 Prague*
[6]*University of Cincinnati, Cincinnati, Ohio 45221*
[7]*Deutsches Elektronen–Synchrotron, 22607 Hamburg*
[8]*Duke University, Durham, North Carolina 27708*
[9]*University of Florida, Gainesville, Florida 32611*
[10]*Key Laboratory of Nuclear Physics and Ion-beam Application (MOE) and Institute of Modern Physics,*
Fudan University, Shanghai 200443
[11]*Justus-Liebig-Universität Gießen, 35392 Gießen*
[12]*Gifu University, Gifu 501-1193*
[13]*II. Physikalisches Institut, Georg-August-Universität Göttingen, 37073 Göttingen*
[14]*SOKENDAI (The Graduate University for Advanced Studies), Hayama 240-0193*
[15]*Gyeongsang National University, Chinju 660-701*
[16]*Hanyang University, Seoul 133-791*
[17]*University of Hawaii, Honolulu, Hawaii 96822*
[18]*High Energy Accelerator Research Organization (KEK), Tsukuba 305-0801*
[19]*J-PARC Branch, KEK Theory Center, High Energy Accelerator Research Organization (KEK),*
Tsukuba 305-0801
[20]*IKERBASQUE, Basque Foundation for Science, 48013 Bilbao, Spain*
[21]*Indian Institute of Technology Bhubaneswar, Satya Nagar 751007*
[22]*Indian Institute of Technology Guwahati, Assam 781039*
[23]*Indian Institute of Technology Hyderabad, Telangana 502285*
[24]*Indian Institute of Technology Madras, Chennai 600036*
[25]*Indiana University, Bloomington, Indiana 47408*

[26]*Institute of High Energy Physics, Chinese Academy of Sciences, Beijing 100049*
[27]*Institute of High Energy Physics, Vienna 1050*
[28]*Institute for High Energy Physics, Protvino 142281*
[29]*INFN—Sezione di Napoli, 80126 Napoli*
[30]*INFN—Sezione di Torino, 10125 Torino*
[31]*Advanced Science Research Center, Japan Atomic Energy Agency, Naka 319-1195*
[32]*J. Stefan Institute, 1000 Ljubljana*
[33]*Kanagawa University, Yokohama 221-8686*
[34]*Institut für Experimentelle Teilchenphysik, Karlsruher Institut für Technologie,*
76131 Karlsruhe
[35]*Kennesaw State University, Kennesaw, Georgia 30144*
[36]*King Abdulaziz City for Science and Technology, Riyadh 11442*
[37]*Department of Physics, Faculty of Science, King Abdulaziz University, Jeddah 21589*
[38]*Korea Institute of Science and Technology Information, Daejeon 305-806*
[39]*Korea University, Seoul 136-713*
[40]*Kyoto University, Kyoto 606-8502*
[41]*Kyungpook National University, Daegu 702-701*
[42]*LAL, Univ. Paris-Sud, CNRS/IN2P3, Université Paris-Saclay, Orsay*
[43]*École Polytechnique Fédérale de Lausanne (EPFL), Lausanne 1015*
[44]*P. N. Lebedev Physical Institute of the Russian Academy of Sciences, Moscow 119991*
[45]*Faculty of Mathematics and Physics, University of Ljubljana, 1000 Ljubljana*
[46]*Ludwig Maximilians University, 80539 Munich*
[47]*Luther College, Decorah, Iowa 52101*
[48]*University of Malaya, 50603 Kuala Lumpur*
[49]*University of Maribor, 2000 Maribor*
[50]*Max-Planck-Institut für Physik, 80805 München*
[51]*School of Physics, University of Melbourne, Victoria 3010*
[52]*University of Mississippi, University, Mississippi 38677*
[53]*University of Miyazaki, Miyazaki 889-2192*
[54]*Moscow Physical Engineering Institute, Moscow 115409*
[55]*Moscow Institute of Physics and Technology, Moscow Region 141700*
[56]*Graduate School of Science, Nagoya University, Nagoya 464-8602*
[57]*Kobayashi-Maskawa Institute, Nagoya University, Nagoya 464-8602*
[58]*Università di Napoli Federico II, 80055 Napoli*
[59]*Nara Women's University, Nara 630-8506*
[60]*National Central University, Chung-li 32054*
[61]*National United University, Miao Li 36003*
[62]*Department of Physics, National Taiwan University, Taipei 10617*
[63]*H. Niewodniczanski Institute of Nuclear Physics, Krakow 31-342*
[64]*Nippon Dental University, Niigata 951-8580*
[65]*Niigata University, Niigata 950-2181*
[66]*University of Nova Gorica, 5000 Nova Gorica*
[67]*Novosibirsk State University, Novosibirsk 630090*
[68]*Osaka City University, Osaka 558-8585*
[69]*Pacific Northwest National Laboratory, Richland, Washington 99352*
[70]*Panjab University, Chandigarh 160014*
[71]*Peking University, Beijing 100871*
[72]*University of Pittsburgh, Pittsburgh, Pennsylvania 15260*
[73]*Theoretical Research Division, Nishina Center, RIKEN, Saitama 351-0198*
[74]*University of Science and Technology of China, Hefei 230026*
[75]*Showa Pharmaceutical University, Tokyo 194-8543*
[76]*Soongsil University, Seoul 156-743*
[77]*Stefan Meyer Institute for Subatomic Physics, Vienna 1090*
[78]*Sungkyunkwan University, Suwon 440-746*
[79]*Department of Physics, Faculty of Science, University of Tabuk, Tabuk 71451*
[80]*Tata Institute of Fundamental Research, Mumbai 400005*
[81]*Excellence Cluster Universe, Technische Universität München, 85748 Garching*
[82]*Department of Physics, Technische Universität München, 85748 Garching*
[83]*Toho University, Funabashi 274-8510*
[84]*Department of Physics, Tohoku University, Sendai 980-8578*

[85]*Earthquake Research Institute, University of Tokyo, Tokyo 113-0032*
[86]*Department of Physics, University of Tokyo, Tokyo 113-0033*
[87]*Tokyo Institute of Technology, Tokyo 152-8550*
[88]*Tokyo Metropolitan University, Tokyo 192-0397*
[89]*Virginia Polytechnic Institute and State University, Blacksburg, Virginia 24061*
[90]*Wayne State University, Detroit, Michigan 48202*
[91]*Yamagata University, Yamagata 990-8560*
[92]*Yonsei University, Seoul 120-749*

The first search for double charged charmoniumlike state production in $\Upsilon(1S)$ and $\Upsilon(2S)$ decays and in e^+e^- annihilation at $\sqrt{s} = 10.52$, 10.58, and 10.867 GeV is conducted using data collected with the Belle detector at the KEKB asymmetric energy electron-positron collider. No significant signals are observed in any of the studied modes, and the 90% credibility level upper limits on their product branching fractions in $\Upsilon(1S)$ and $\Upsilon(2S)$ decays [$\mathcal{B}(\Upsilon(1S, 2S) \to Z_c^+ Z_c^{(\prime)-}) \times \mathcal{B}(Z_c^+ \to \pi^+ + c\bar{c})$ ($c\bar{c} = J/\psi, \chi_{c1}(1P)$, $\psi(2S)$)] and the product of Born cross section and branching fraction for $e^+e^- \to Z_c^+ Z_c^{(\prime)-}$ ($\sigma(e^+e^- \to Z_c^+ Z_c^{(\prime)-}) \times \mathcal{B}(Z_c^+ \to \pi^+ + c\bar{c})$) at $\sqrt{s} = 10.52$, 10.58, and 10.867 GeV are determined. Here, Z_c refers to the $Z_c(3900)$ and $Z_c(4200)$ observed in the $\pi J/\psi$ final state, the $Z_{c1}(4050)$ and $Z_{c2}(4250)$ in the $\pi \chi_{c1}(1P)$ final state, and the $Z_c(4050)$ and $Z_c(4430)$ in the $\pi \psi(2S)$ final state.

I. INTRODUCTION

In the past decade, many experiments, at both lepton and hadron colliders, reported evidence for a large number of new particles having exotic properties that are difficult to accommodate within the conventional quark model, especially those that couple to heavy quarkonium and have nonzero charge [1]. Since the discovery of the $Z_c^+(4430)(\to \pi^+ \psi(2S))$ [2], more charged charmoniumlike resonances have been observed, including $Z_{c1}^+(4050)$ and $Z_{c2}^+(4250)(\to \pi^+ \chi_{c1}(1P))$ [3], $Z_c^+(3900)$ [4,5] and $Z_c^+(4200)(\to \pi^+ J/\psi)$ [6], and $Z_c^+(4050)(\to \pi^+ \psi(2S))$ [7]. The preferred assignment of the quantum numbers for $Z_c^+(4430)$, $Z_c^+(3900)$, and $Z_c^+(4200)$ are $J^P = 1^+$ [6,8,9]. Although these charged charmoniumlike candidates are widely interpreted unconventional $c\bar{c}$ states, it remains a significant challenge to determine their internal dynamics [10].

Considerable efforts in theory have been devoted to interpreting these states as tetraquarks, molecules, hybrids, or hadrocharmonia [11–13]. To distinguish among these explanations, experimental input is needed, such as that from the study of double $Z_c^\pm$ production in e^+e^- annihilation [14,15]. For $e^+e^- \to Z_c^+ Z_c^-$, the dependence on s (the e^+e^- c.m. energy squared) of the electromagnetic form factor, $F_{Z_c^+ Z_c^-}$, is $1/s^3$ for a Z_c state with tetraquark

structure or $1/s$ for a Z_c system of two tightly bound diquarks [14,15].

In this paper, we report the search for Z_c-pair production in $\Upsilon(1S)$ and $\Upsilon(2S)$ decays as well as in e^+e^- annihilation at $\sqrt{s} = 10.52$, 10.58, and 10.867 GeV. We measure the production rates of $\Upsilon(1S)$ and $\Upsilon(2S)$ decay into a pair of Z_c states and the Born cross sections of $e^+e^- \to Z_c^+ Z_c^{(\prime)-}$ at $\sqrt{s} = 10.52$, 10.58, and 10.867 GeV. Here, Z_c^+ denotes $Z_c^+(3900)$, $Z_c^+(4200)$, $Z_{c1}^+(4050)$, $Z_{c2}^+(4250)$, $Z_c^+(4050)$, or $Z_c^+(4430)$. In these searches, the decay modes considered are $Z_c^+(3900)/Z_c^+(4200) \to \pi^+ J/\psi$, $Z_{c1}^+(4050)/Z_{c2}^+(4250) \to \pi^+ \chi_{c1}(1P)$, and $Z_c^+(4050)/Z_c^+(4430) \to \pi^+ \psi(2S)$ [16]. Although it is possible to search for combinations of any two of the enumerated Z_c states, only both Z_c states decaying into the same final states are currently studied in this study; the information of the other final-state combinations can be estimated from the results reported here.

II. DATA SAMPLE AND THE BELLE DETECTOR

This analysis utilizes (5.74 ± 0.09) fb^{-1} data collected at the $\Upsilon(1S)$ peak [(102 ± 3) million $\Upsilon(1S)$ events], (24.91 ± 0.35) fb^{-1} data collected at the $\Upsilon(2S)$ peak [(158 ± 4) million $\Upsilon(2S)$ events], (89.5 ± 1.3) fb^{-1} data collected at $\sqrt{s} = 10.52$ GeV, (711.0 ± 10.0) fb^{-1} data collected at $\sqrt{s} = 10.58$ GeV [$\Upsilon(4S)$ peak], and (121.4 ± 1.7) fb^{-1} data collected at $\sqrt{s} = 10.867$ GeV [$\Upsilon(5S)$ peak]. All the data were collected with the Belle detector [17] operating at the KEKB asymmetric-energy e^+e^- collider [18]. The Belle detector is a large solid-angle magnetic spectrometer that consists of a silicon vertex detector, a 50-layer central drift chamber (CDC), an array

TABLE I.   The world-average (nominal) values of $Z_c^\pm$ masses (in MeV/c^2) and widths (in MeV) [23].

Z_c states	Z_c labels in Ref. [23]	Mass	Width
$Z_c^+(3900)$	$X^+(3900)$	3886.6 ± 2.4	28.1 ± 2.6
$Z_c^+(4200)$	$X^+(4200)$	4196^{+35}_{-32}	370^{+100}_{-150}
$Z_{c1}^+(4050)$	$X^+(4050)$	4051^{+24}_{-40}	82^{+50}_{-28}
$Z_{c2}^+(4250)$	$X^+(4250)$	4248^{+190}_{-50}	177^{+320}_{-70}
$Z_c^+(4050)$	$X^+(4055)$	4054 ± 3.2	45 ± 13
$Z_c^+(4430)$	$X^+(4430)$	4478^{+15}_{-18}	181 ± 31

of aerogel threshold Cherenkov counters (ACC), a barrel-like arrangement of time-of-flight scintillation counters (TOF), and an electromagnetic calorimeter comprised of CsI(TI) crystals (ECL) located inside a superconducting solenoid coil that provides a $1.5T$ magnetic field. An iron flux-return yoke instrumented with resistive plate chambers located outside the coil is used to detect K_L^0 mesons and to identify muons. A detailed description of the Belle detector can be found in Refs. [17,19].

We generate large signal Monte Carlo (MC) samples with the EVTGEN event generator [20] to understand the signal event topology and to estimate the signal selection efficiency. The angular distribution for $\Upsilon(1S, 2S) \rightarrow Z_c^+ Z_c^{(\prime)-}$ and $e^+e^- \rightarrow Z_c^+ Z_c^{(\prime)-}$ at $\sqrt{s} = 10.52$, 10.58, and 10.867 GeV is simulated assuming an $e^+e^- \rightarrow A\bar{A}$ decay mode (A denoting an axial-vector state), i.e., $dN/d\cos\theta_{Z_c} \propto 1 - \cos^2\theta_{Z_c}$ [21], where θ_{Z_c} is the polar angle of the Z_c in the e^+e^- c.m. system. Initial-state radiation (ISR) is taken into account by assuming that the cross sections follow a $1/s^2$ dependence in $e^+e^- \rightarrow Z_c^+ Z_c^{(\prime)-}$ reactions. For the Z_c pair in one MC event, one Z_c decays into $\pi^\pm J/\psi$, $\pi^\pm\chi_{c1}(1P)$, or $\pi^\pm\psi(2S)$ using the phase space model, while the other is simulated with the inclusive decays using PYTHIA [22]. The masses and widths of the $Z_c^\pm$ states are set according to the latest world-average values [23], as summarized in Table I.

III. COMMON EVENT SELECTION CRITERIA

For well-reconstructed charged tracks, the impact parameters perpendicular to and along the beam direction with respect to the nominal interaction point are required to be less than 0.5 and 4 cm, respectively, and the transverse momentum in the laboratory frame is required to be larger than 0.1 GeV/c. We require the number of well-reconstructed charged tracks to be greater than four to suppress the significant background from quantum electro-dynamics processes. For charged tracks, information from different detector subsystems including specific ionization in the CDC, time measurements in the TOF, and the response of the ACC is combined to form the likelihood $\mathcal{L}_i$ for particle species i, where $i = \pi$, K, or p [24]. Charged tracks with $R_K = \mathcal{L}_K/(\mathcal{L}_K + \mathcal{L}_\pi) < 0.4$ are considered to be pions. With this condition, the pion identification

efficiency is 97%, and the kaon to pion misidentification rate is about 4%. A similar likelihood ratio is defined as $R_e = \mathcal{L}_e/(\mathcal{L}_e + \mathcal{L}_{\text{non}-e})$ [25] for electron identification and $R_\mu = \mathcal{L}_\mu/(\mathcal{L}_\mu + \mathcal{L}_K + \mathcal{L}_\pi)$ [26] for muon identification. An ECL cluster is treated as a photon candidate if it is isolated from the projected path of charged tracks in the CDC, and its energy is greater than 50 MeV.

For the lepton pair $\ell^+\ell^-$ ($\ell = e$ or μ) used to reconstruct the J/ψ, both tracks must have $R_e > 0.95$ in the e^+e^- mode, while one track must have $R_\mu > 0.95$ and the other $R_\mu > 0.05$ in the $\mu^+\mu^-$ mode. The lepton-pair identification efficiencies for e^+e^- and $\mu^+\mu^-$ are 96% and 93%, respectively. We apply a lepton veto to the bachelor pion candidate by requiring $R_\mu < 0.95$ and $R_e < 0.95$. To reduce the effect of bremsstrahlung and final-state radiation, photons detected in the ECL within a 50 mrad cone of the original electron or positron direction are absorbed into the e^+/e^- four-momentum.

IV. SEARCH FOR $\Upsilon(1S, 2S) \rightarrow Z_c^+ Z_c^{(\prime)-}$ AND $e^+e^- \rightarrow Z_c^+ Z_c^{(\prime)-}$ AT $\sqrt{s} = 10.52$, 10.58, AND 10.867 GEV WITH $Z_c^+ \rightarrow \pi^+ J/\psi$

We search for the production of double-$Z_c(3900)$ states, double-$Z_c(4200)$ states, and $Z_c(3900)$-plus-$Z_c(4200)$ states in $\Upsilon(1S, 2S)$ decays and e^+e^- annihilation at $\sqrt{s} = 10.52$, 10.58, and 10.867 GeV, where one Z_c decays into π^+ and J/ψ ($\rightarrow \ell^+\ell^-$) and the other decays inclusively.

After applying the aforementioned common event selections, the invariant-mass distributions of the J/ψ candidates from the five data samples are shown in Figs. 1(a)–1(e). Clear J/ψ signals are observed. The J/ψ signal region is defined as $|M_{\ell^+\ell^-} - m_{J/\psi}| < 0.03$ GeV/c^2 (> 98% signal events are reserved according to the MC simulation), where $m_{J/\psi}$ is the nominal mass [23], while the J/ψ mass sidebands are $2.97 < M_{\ell^+\ell^-} < 3.03$ GeV/c^2 or $3.17 < M_{\ell^+\ell^-} < 3.23$ GeV/c^2 (twice the width of the signal region). In order to improve the J/ψ momentum resolution, a mass-constrained fit is applied to the J/ψ candidates in the signal region.

For the events with the lepton-pair mass within the J/ψ signal region, Figs. 2(a)–2(c) show the recoil-mass spectra of the $Z_c^+(\rightarrow \pi^+ J/\psi)$ states from $\Upsilon(1S)$ decays in signal MC samples. The Z_c^+ shapes are described by Breit-Wigner (BW) functions convolved with Gaussian functions. The solid arrows show the required recoil-mass signal region.

To suppress the background level effectively for $\Upsilon(1S)$ decays, we require the recoil mass of $\pi^+ J/\psi$, $M_{\text{miss}}(\pi^+ J/\psi)$, to satisfy $|M_{\text{miss}}(\pi^+ J/\psi) - m_{Z_c^-(3900)}| < 0.03$ GeV/c^2 for the double-$Z_c(3900)$ mode or $|M_{\text{miss}}(\pi^+ J/\psi) - m_{Z_c^-(4200)}| < 0.21$ GeV/c^2 for the double-$Z_c(4200)$ and $Z_c(3900)$-plus-$Z_c(4200)$ modes, where $m_{Z_c^-(3900)}$ and $m_{Z_c^-(4200)}$ are the nominal masses [23] and

$$M_{\text{miss}}(\pi^+ J/\psi) = \sqrt{(p_{e^+e^-} - p_{\pi^+ J/\psi})^2}$$ ($p_{e^+e^-}$ and $p_{\pi^+ J/\psi}$
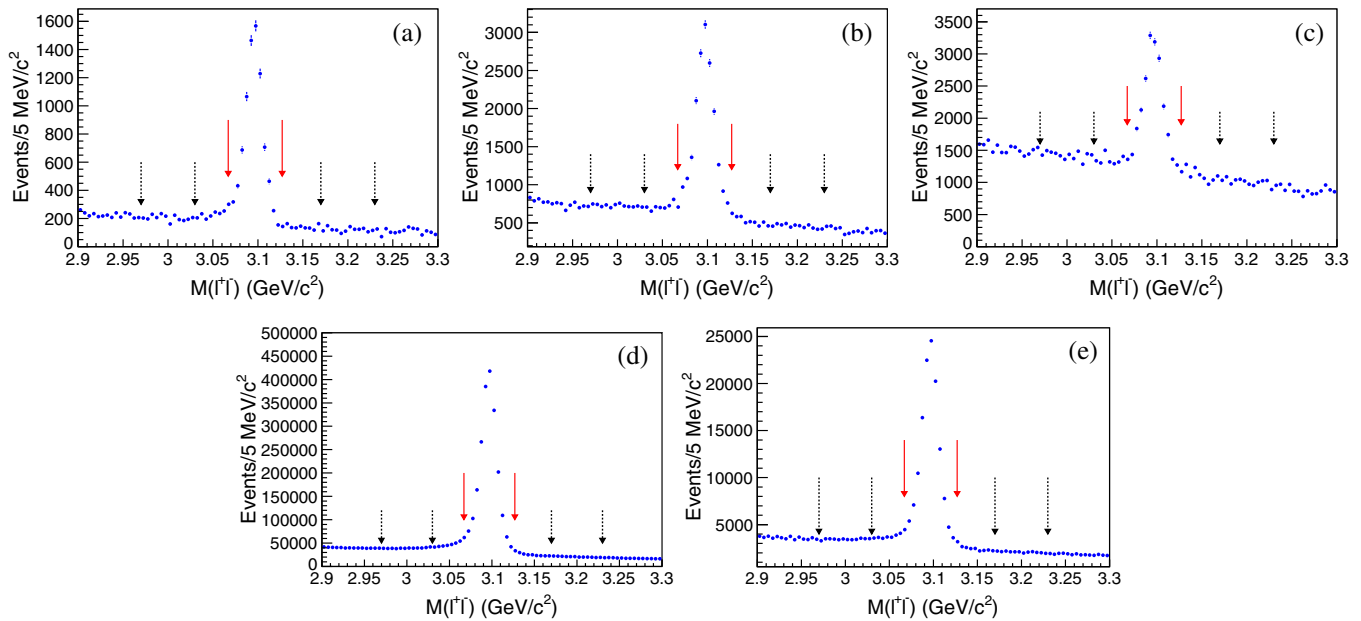
FIG. 1. The invariant-mass distributions of the J/ψ candidates from (a) $\Upsilon(1S)$, (b) $\Upsilon(2S)$, (c) $\sqrt{s} = 10.52$ GeV, (d) $\sqrt{s} = 10.58$ GeV, and (e) $\sqrt{s} = 10.867$ GeV data samples. The solid red arrows show the J/ψ signal region, and the dashed black arrows show the J/ψ mass sideband regions.

are the four-momenta of the e^+e^- and π^+J/ψ systems). These requirements maximize $S/\sqrt{S+B}$, where S is the number of fitted signal events in signal MC samples assuming $\mathcal{B}(\Upsilon(1S) \to Z_c^+Z_c^{(\prime)-}) \times \mathcal{B}(Z_c^+ \to \pi^+J/\psi) = 10^{-5}$ and B is the number of estimated background events in the Z_c^+ signal region using inclusive MC samples. The same requirements also maximize $S/\sqrt{S+B}$ for $\Upsilon(2S)$ decays and e^+e^- reactions at $\sqrt{s} = 10.52$, 10.58, and 10.867 GeV.

After the application of the above requirements, Figs. 3(a)–3(c) show the invariant-mass distributions of the Z_c^+ states from $\Upsilon(1S)$ decays in the MC signal sample, where the solid lines show the fitted results with a BW function convolved with a Gaussian function as Z_c^+ signal shapes. Here, all combinations of π^+J/ψ are retained, as is done for the modes $\pi^+\chi_{c1}$ and $\pi^+\psi(2S)$. Fewer than 1% of events have multiple entries here. Based on the fitted

results, the signal selection efficiencies are obtained and listed in Table II. Note that the efficiencies of the double-$Z_c(3900)$ and double-$Z_c(4200)$ modes are determined from the sum of the reconstructed Z_c^+ and Z_c^- signals. This applies as well for double-Z_c production in the other data sets with the same Z_c.

Figures 4(a)–4(o) show the π^+J/ψ invariant-mass spectra from the five data samples together with the backgrounds from the normalized J/ψ mass sideband events. There are no evident signals for Z_c^+ states at the expected positions. No peaking backgrounds are found in the J/ψ mass sideband events or in the $\Upsilon(1S, 2S)$ and $e^+e^- \to q\bar{q}$ ($q = u$, d, s, c) inclusive MC samples. There is a wide background enhancement at around 4.5 GeV/c^2 in the π^+J/ψ invariant-mass distribution for $e^+e^- \to Z_c^+(4200)Z_c^-(4200)$ at $\sqrt{s} = 10.58$ GeV, as shown in Fig. 4(k), arising from B decays to a J/ψ meson.
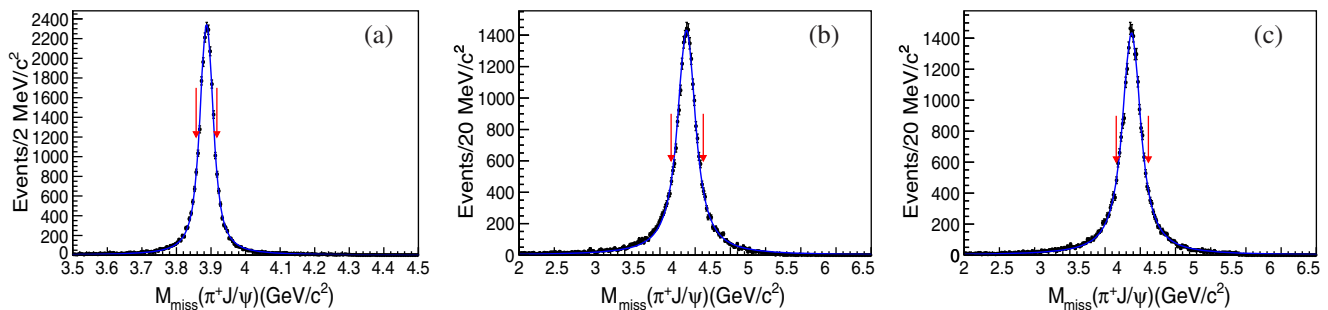

FIG. 2. The recoil-mass spectra of the Z_c^+ ($\to \pi^+J/\psi$) states from MC simulated (a) $\Upsilon(1S) \to Z_c^+(3900)Z_c^-(3900)$, (b) $\Upsilon(1S) \to Z_c^+(4200)Z_c^-(4200)$, and (c) $\Upsilon(1S) \to Z_c^+(3900)Z_c^-(4200) +$ c.c.
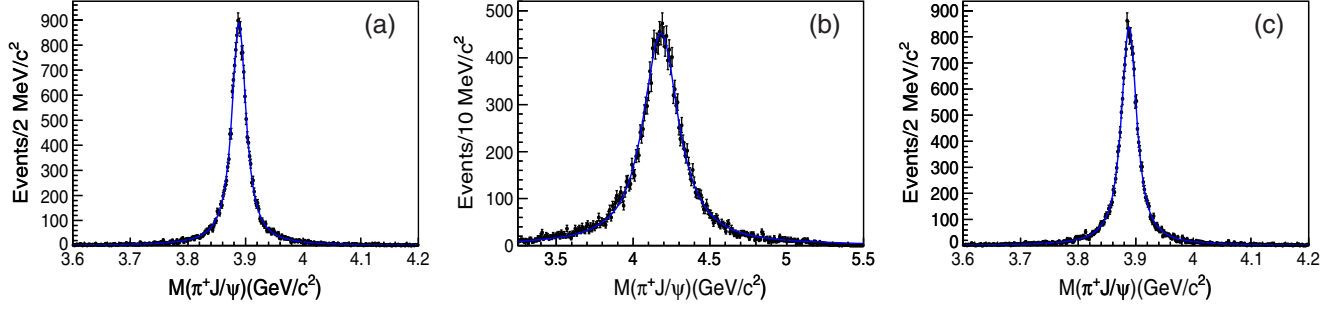
FIG. 3. The invariant-mass distributions of the Z_c^+ ($\to \pi^+ J/\psi$) states from MC simulated (a) $\Upsilon(1S) \to Z_c^+(3900)Z_c^-(3900)$, (b) $\Upsilon(1S) \to Z_c^+(4200)Z_c^-(4200)$, and (c) $\Upsilon(1S) \to Z_c^+(3900)Z_c^-(4200) +$ c.c.

Although these background events can be removed by requiring that the J/ψ momentum in the e^+e^- c.m. frame be larger than 2.5 GeV/c ($P^*_{J/\psi} > 2.5$ GeV/c), we retain them since the requirement of $P^*_{J/\psi} > 2.5$ GeV/c decreases the signal efficiency by 40%, and this distinct feature is well described by a third-order Chebyshev polynomial function.

An unbinned extended maximum likelihood fit to each $\pi^+ J/\psi$ invariant-mass spectrum is performed to extract the signal and background yields in the five data samples. The Z_c^+ signal shapes used in the fits are BW functions

convolved with a Gaussian function as signal probability density functions [the parameters of the BW function being fixed to the nominal masses and widths of Z_c^+ states and Gaussian functions being fixed to those from the fits to MC signal samples with mass resolutions of 4 and 6 MeV/c^2 for $Z_c^+(3900)$ and $Z_c^+(4200)$, respectively]. For the backgrounds, a second-order Chebyshev polynomial function is adopted, except for $e^+e^- \to Z_c^+(4200)Z_c^-(4200)$ at $\sqrt{s} = 10.58$ GeV, where a third-order polynomial is used. The fitted results are shown in Fig. 4 and summarized in Tables II and III.

TABLE II. Summary of the 90% C.L. upper limits on $\mathcal{B}(\Upsilon(1S, 2S) \to Z_c^+ Z_c^{(\prime)-}) \times \mathcal{B}(Z_c^+ \to \pi^+ J/\psi)$ for $Z_c^+(3900)Z_c^-(3900)$, $Z_c^+(4200)Z_c^-(4200)$, and $Z_c^+(3900)Z_c^-(4200) +$ c.c., where N^{fit} is the signal yield, N^{UL} is the 90% C.L. upper limit on the number of signal events, $\varepsilon(\%)$ is the selection efficiency, $\Sigma(\sigma)$ is the statistical signal significance, $\sigma_{\text{syst}}(\%)$ is the total systematic uncertainty, and $\mathcal{B}$ and $\mathcal{B}^{\text{UL}}$ are the branching fraction and the corresponding 90% C.L. upper limit on the branching fraction in units of 10^{-6}.

Mode	N^{fit}	N^{UL}	$\varepsilon(\%)$	$\Sigma(\sigma)$	$\sigma_{\text{syst}}(\%)$	$\mathcal{B}(\Upsilon \to Z_c^+ Z_c^{(\prime)-}) \times$ $\mathcal{B}(Z_c^+ \to \pi^+ J/\psi)$	$\mathcal{B}^{\text{UL}}(\Upsilon \to Z_c^+ Z_c^{(\prime)-}) \times$ $\mathcal{B}(Z_c^+ \to \pi^+ J/\psi)$
$\Upsilon(1S) \to Z_c^+(3900)Z_c^-(3900)$	0.9 ± 4.3	9.2	44.1	0.2	25.2	0.2 ± 0.7	1.8
$\Upsilon(1S) \to Z_c^+(4200)Z_c^-(4200)$	50.9 ± 42.4	117.1	44.6	1.2	27.8	9.4 ± 8.3	22.3
$\Upsilon(1S) \to Z_c^+(3900)Z_c^-(4200) +$ c.c.	3.0 ± 10.1	22.0	22.6	0.3	20.5	1.1 ± 3.7	8.1
$\Upsilon(2S) \to Z_c^+(3900)Z_c^-(3900)$	-1.7 ± 3.0	7.4	41.1	$\cdots$	16.9	-0.2 ± 0.4	1.0
$\Upsilon(2S) \to Z_c^+(4200)Z_c^-(4200)$	58.0 ± 47.9	125.2	42.2	1.2	31.4	7.3 ± 6.4	16.7
$\Upsilon(2S) \to Z_c^+(3900)Z_c^-(4200) +$ c.c.	11.2 ± 11.5	29.2	21.3	1.0	16.8	2.8 ± 2.9	7.3

TABLE III. Summary of the 90% C.L. upper limits on $\sigma(e^+e^- \to Z_c^+ Z_c^{(\prime)-}) \times \mathcal{B}(Z_c^+ \to \pi^+ J/\psi)$ for $Z_c^+(3900)Z_c^-(3900)$, $Z_c^+(4200)Z_c^-(4200)$, and $Z_c^+(3900)Z_c^-(4200) +$ c.c. at $\sqrt{s} = 10.52$, 10.58, and 10.867 GeV, where N^{fit} is the signal yield, N^{UL} is the 90% C.L. upper limit on the number of signal events, $\varepsilon(\%)$ is the selection efficiency, $\Sigma(\sigma)$ is the statistical signal significance, $\sigma_{\text{syst}}(\%)$ is the total systematic uncertainty, σ is the Born cross section $\sigma(e^+e^- \to Z_c^+ Z_c^{(\prime)-})$, and σ^{UL} is the corresponding 90% C.L. upper limit in units of fb.

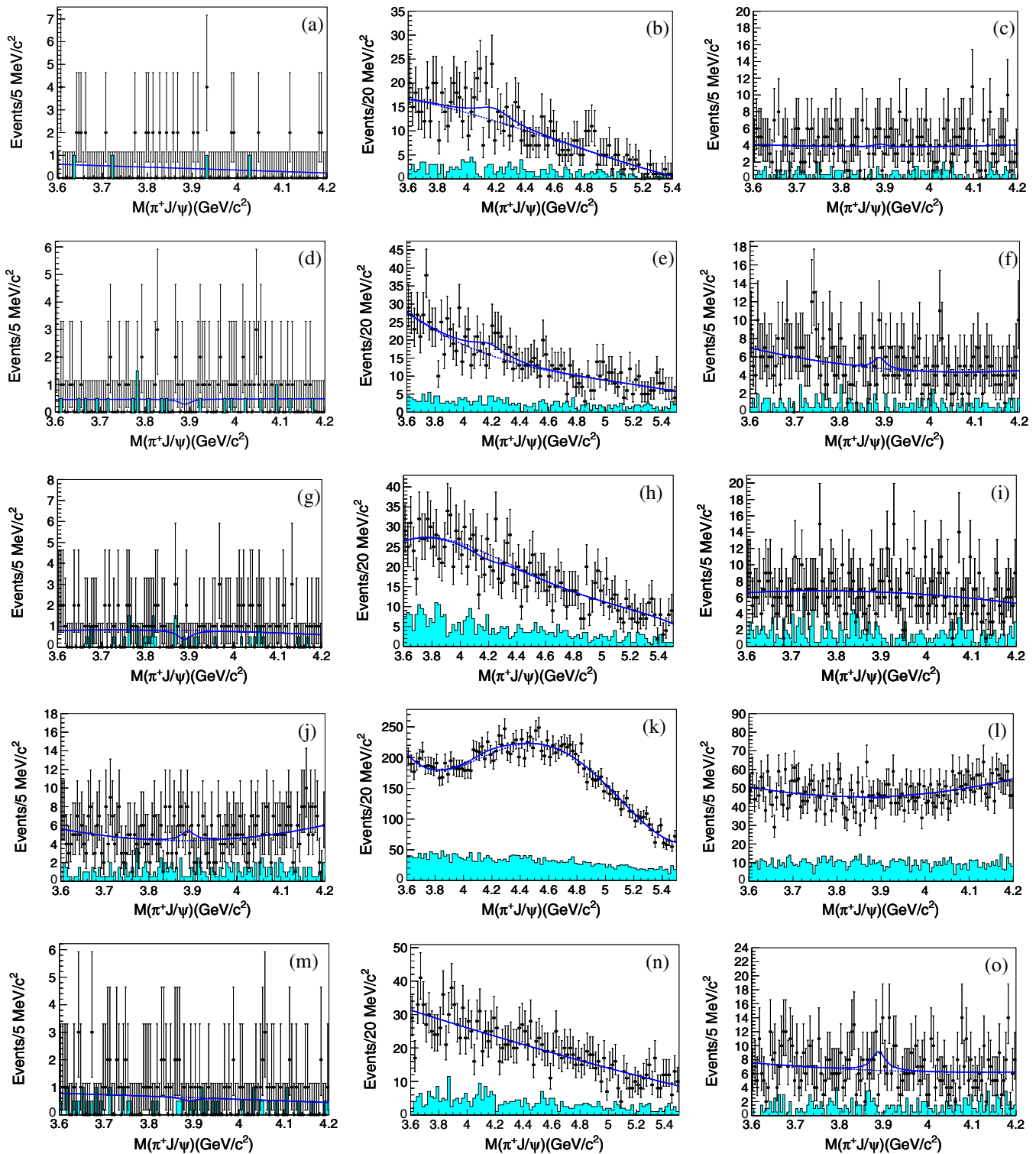| Mode	$\sqrt{s}$ (GeV)	N^{fit}	N^{UL}	$\varepsilon(\%)$	$\Sigma(\sigma)$	$\sigma_{\text{syst}}(\%)$	$\sigma \times \mathcal{B}(Z_c^+ \to \pi^+ J/\psi)$	$\sigma^{\text{UL}} \times \mathcal{B}(Z_c^+ \to \pi^+ J/\psi)$
$e^+e^- \to Z_c^+(3900)Z_c^-(3900)$	10.52	-4.9 ± 3.6	7.2	41.5	$\cdots$	10.3	-1.6 ± 1.2	2.3
$e^+e^- \to Z_c^+(4200)Z_c^-(4200)$	10.52	-27.5 ± 57.8	82.8	43.7	$\cdots$	34.2	-8.5 ± 18.1	26.5
$e^+e^- \to Z_c^+(3900)Z_c^-(4200) +$ c.c.	10.52	-0.5 ± 15.0	28.4	21.0	$\cdots$	22.9	-0.3 ± 9.7	18.3
$e^+e^- \to Z_c^+(3900)Z_c^-(3900)$	10.58	11.8 ± 13.0	32.2	41.5	0.9	12.7	0.5 ± 0.5	1.3
$e^+e^- \to Z_c^+(4200)Z_c^-(4200)$	10.58	132.1 ± 173.0	390.1	43.4	0.8	35.4	5.1 ± 6.9	15.5
$e^+e^- \to Z_c^+(3900)Z_c^-(4200) +$ c.c.	10.58	-7.7 ± 39.4	63.4	20.8	$\cdots$	20.7	-0.6 ± 3.2	5.1
$e^+e^- \to Z_c^+(3900)Z_c^-(3900)$	10.867	-1.4 ± 4.6	9.0	41.5	$\cdots$	17.0	-0.3 ± 1.1	2.2
$e^+e^- \to Z_c^+(4200)Z_c^-(4200)$	10.867	-0.2 ± 41.6	93.7	43.7	$\cdots$	33.2	-0.1 ± 9.4	21.9
$e^+e^- \to Z_c^+(3900)Z_c^-(4200) +$ c.c.	10.867	30.3 ± 16.7	53.9	20.5	1.9	16.3	14.6 ± 8.4	26.6

FIG. 4.   The invariant-mass spectra of the Z_c^+ ($\rightarrow \pi^+ J/\psi$) states in the processes (a) $\Upsilon(1S) \rightarrow Z_c^+(3900)Z_c^-(3900)$; (b) $\Upsilon(1S) \rightarrow Z_c^+(4200)Z_c^-(4200)$; (c) $\Upsilon(1S) \rightarrow Z_c^+(3900)Z_c^-(4200) +$ c.c.; (d) $\Upsilon(2S) \rightarrow Z_c^+(3900)Z_c^-(3900)$; (e) $\Upsilon(2S) \rightarrow Z_c^+(4200)Z_c^-(4200)$; (f) $\Upsilon(2S) \rightarrow Z_c^+(3900)Z_c^-(4200) +$ c.c.; (g)–(i) $e^+e^- \rightarrow Z_c^+(3900)Z_c^-(3900)$, $e^+e^- \rightarrow Z_c^+(4200)Z_c^-(4200)$, and $e^+e^- \rightarrow Z_c^+(3900)Z_c^-(4200) +$ c.c. at $\sqrt{s} = 10.52$ GeV; (j)–(l) $e^+e^- \rightarrow Z_c^+(3900)Z_c^-(3900)$, $e^+e^- \rightarrow Z_c^+(4200)Z_c^-(4200)$, and $e^+e^- \rightarrow Z_c^+(3900)Z_c^-(4200) +$ c.c. at $\sqrt{s} = 10.58$ GeV; and (m)–(o) $e^+e^- \rightarrow Z_c^+(3900)Z_c^-(3900)$, $e^+e^- \rightarrow Z_c^+(4200)Z_c^-(4200)$, and $e^+e^- \rightarrow Z_c^+(3900)Z_c^-(4200) +$ c.c. at $\sqrt{s} = 10.867$ GeV. The solid curves are the best fits described in the text, the dotted lines are the fitted backgrounds, and the shaded histograms are from the normalized J/ψ mass sideband events.

The $\mathcal{B}(\Upsilon(1S,2S) \to Z_c^+ Z_c^{(\prime)-}) \times \mathcal{B}(Z_c^+ \to \pi^+ J/\psi)$ and $\sigma(e^+e^- \to Z_c^+ Z_c^{(\prime)-}) \times \mathcal{B}(Z_c^+ \to \pi^+ J/\psi)$ are calculated using

$$\frac{N_{\text{fit}}}{N_{\Upsilon(1S,2S)} \times \varepsilon \times \mathcal{B}_{\text{decay}}} \tag{1}$$

and

$$\frac{N_{\text{fit}} \times |1 - \prod|^2}{\mathcal{L} \times \mathcal{B}_{\text{decay}} \times \varepsilon \times (1 + \delta)_{\text{ISR}}}, \tag{2}$$

respectively, where N_{fit} is the fitted Z_c^+ signal yield, $N_{\Upsilon(1S,2S)}$ is the total number of $\Upsilon(1S,2S)$ events, ε is the corresponding selection efficiency, $\mathcal{L}$ is the integrated luminosity, $\mathcal{B}_{\text{decay}} = \mathcal{B}(J/\psi \to \ell^+\ell^-)$ [23], $(1 + \delta)_{\text{ISR}}$ is the radiative correction factor, and $|1 - \prod|^2$ is the vacuum polarization factor. The radiative correction factors $(1 + \delta)_{\text{ISR}}$ are 0.650, 0.657, and 0.654 for $\sqrt{s} = 10.52$, 10.58, and 10.867 GeV, respectively, calculated using formulas given in Ref. [27]; the corresponding values of $|1 - \prod|^2$ are 0.931, 0.930, and 0.929 [28]. In the calculation of $(1 + \delta)_{\text{ISR}}$, we assume that the s dependence of the cross section is $\sigma(e^+e^- \to A\bar{A}) \propto 1/s^2$. The product branching fractions and the product of the Born cross section and the branching fraction for the studied modes are listed in Tables II and III.

The statistical significances of the Z_c^+ signals are calculated using $\sqrt{-2\ln(\mathcal{L}_0/\mathcal{L}_{\text{max}})}$, where $\mathcal{L}_0$ and $\mathcal{L}_{\text{max}}$ are the likelihoods of the fits without and with signal, respectively. The values are summarized in Tables II and III. Since the statistical significance in each case is less than 3σ, upper limits on the signal yields (N^{UL}), the product branching fractions [$\mathcal{B}^{\text{UL}}(\Upsilon(1S,2S) \to Z_c^+ Z_c^{(\prime)-}) \times \mathcal{B}(Z_c^+ \to \pi^+ J/\psi)$], and the product of the Born cross section and the branching fraction [$\sigma^{\text{UL}}(e^+e^- \to Z_c^+ Z_c^{(\prime)-}) \times \mathcal{B}(Z_c^+ \to \pi^+ J/\psi)$], are determined at the 90% credibility level (C.L.) [29] by solving the equation $\int_0^{x^{\text{UL}}} \mathcal{L}(x)dx / \int_0^{+\infty} \mathcal{L}(x)dx = 0.9$, where x is the assumed signal yield, product branching fraction, or product of the Born cross section and the branching fraction and $\mathcal{L}(x)$ is the corresponding maximized likelihood for the data. To take into account the systematic uncertainties discussed in Sec. VI, the likelihood is convolved with a Gaussian function of which the width equals the corresponding systematic uncertainty.

The determined 90% C.L. upper limits of N^{UL}, $\mathcal{B}^{\text{UL}}(\Upsilon(1S,2S) \to Z_c^+ Z_c^{(\prime)-}) \times \mathcal{B}(Z_c^+ \to \pi^+ J/\psi)$, and $\sigma^{\text{UL}}(e^+e^- \to Z_c^+ Z_c^{(\prime)-}) \times \mathcal{B}(Z_c^+ \to \pi^+ J/\psi)$ at $\sqrt{s} = 10.52$, 10.58, and 10.867 GeV are listed in Tables II and III, together with the signal yields (N^{fit}), the selection efficiencies (ε), the statistical significances (Σ), the systematic uncertainties (σ_{syst}) (discussed below), and the central values of $\mathcal{B}(\Upsilon(1S,2S) \to Z_c^+ Z_c^{(\prime)-}) \times \mathcal{B}(Z_c^+ \to \pi^+ J/\psi)$ and $\sigma(e^+e^- \to Z_c^+ Z_c^{(\prime)-}) \times \mathcal{B}(Z_c^+ \to \pi^+ J/\psi)$, with the total errors being the sum in quadrature of the statistical and systematic errors.

V. SEARCH FOR $\Upsilon(1S,2S) \to Z_c^+ Z_c^{(\prime)-}$ AND $e^+e^- \to Z_c^+ Z_c^{(\prime)-}$ AT $\sqrt{s} = 10.52$, 10.58, AND 10.867 GEV WITH $Z_c^+ \to \pi^+ \chi_{c1}(1P), \pi^+ \psi(2S)$

In the five data sets, we search for the production of double-$Z_{c1}(4050)$ states, double-$Z_{c2}(4250)$ states, and $Z_{c1}(4050)$-plus-$Z_{c2}(4250)$ states, where one of the Z_c decays into π^+ and $\chi_{c1}(1P)$ and the other decays inclusively, and double-$Z_c(4050)$ states, double-$Z_c(4430)$ states, and $Z_c(4050)$-plus-$Z_c(4430)$ states, where one of the Z_c decays into π^+ and $\psi(2S)$ and the other decays inclusively. The $\chi_{c1}(1P)$ and $\psi(2S)$ are reconstructed via their decays into $\gamma J/\psi$ and $\pi^+\pi^- J/\psi$, respectively, with $J/\psi \to \ell^+\ell^-$.

After requiring the mass of the lepton pair to be within the J/ψ signal region ($|M_{\ell^+\ell^-} - m_{J/\psi}| < 0.03$ GeV/c^2), Figs. 5(a)–5(e) and 6(a)–6(e) show the invariant-mass distributions of the $\chi_{c1}(1P)$ and $\psi(2S)$ candidates from five data samples. Clear $\chi_{c1}(1P)$ signals could be seen in $\Upsilon(1S)$ decay and in e^+e^- annihilation at $\sqrt{s} = 10.58$ and 10.867 GeV, and evidence for $\chi_{c1}(1P)$ is observed in $\Upsilon(2S)$ decay; clear $\psi(2S)$ signals are observed in $\Upsilon(1S,2S)$ decay and in e^+e^- annihilation at $\sqrt{s} = 10.52$, 10.58, and 10.867 GeV. We define the $\chi_{c1}(1P)$ and $\psi(2S)$ signal and sideband regions as follows. The $\chi_{c1}(1P)$ signal region is $|M_{\gamma J/\psi} - m_{\chi_{c1}(1P)}| < 0.04$ GeV/c^2 ($> 98\%$ signal events are reserved according to the MC simulation), where $m_{\chi_{c1}(1P)}$ is the nominal mass [23], while the $\chi_{c1}(1P)$ mass sidebands are $3.35 < M_{\gamma J/\psi} < 3.43$ GeV/c^2 or $3.62 < M_{\gamma J/\psi} < 3.70$ GeV/c^2 (twice the width of the signal region). The $\psi(2S)$ signal region is $|M_{\pi^+\pi^- J/\psi} - m_{\psi(2S)}| < 0.007$ GeV/c^2 ($> 98\%$ signal events are reserved according to the MC simulation), where $m_{\psi(2S)}$ is the nominal mass [23], while the $\psi(2S)$ mass sidebands are $3.65 < M_{\pi^+\pi^- J/\psi} < 3.664$ GeV/c^2 or $3.71 < M_{\pi^+\pi^- J/\psi} < 3.724$ GeV/c^2 (twice the width of the signal region).

As before, for $\Upsilon(1S)$ decays, we optimize the requirements of recoil mass of $\pi^+\chi_{c1}(1P)$ and $\pi^+\psi(2S)$ by maximizing $S/\sqrt{S+B}$. The optimized requirements are $|M_{\text{miss}}(\pi^+\chi_{c1}(1P)) - m_{Z_{c1}^-(4050)}| < 0.08$ GeV/c^2 for the $Z_{c1}^+(4050)Z_{c1}^-(4050)$ mode and $|M_{\text{miss}}(\pi^+\chi_{c1}(1P)) - m_{Z_{c2}^-(4250)}| < 0.13$ GeV/c^2 for the $Z_{c2}^+(4250)Z_{c2}^-(4250)$ and $Z_{c1}^+(4050)Z_{c2}^-(4250) + $ c.c. modes; they are $|M_{\text{miss}}(\pi^+\psi(2S)) - m_{Z_c^-(4050)}| < 0.06$ GeV/c^2 for the $Z_c^+(4050)Z_c^-(4050)$ mode and $|M_{\text{miss}}(\pi^+\psi(2S)) - m_{Z_c^-(4430)}| < 0.12$ GeV for the $Z_c^+(4430)Z_c^-(4430)$ and $Z_c^+(4050)Z_c^-(4430) + $ c.c. modes. For $\Upsilon(2S)$ decays and e^+e^- reactions at $\sqrt{s} = 10.52$, 10.58, and 10.867 GeV, the optimized requirements are the same as $\Upsilon(1S)$.

After the application of these requirements, Figs. 7(a)–7(o) and 8(a)–8(o) show the $\pi^+\chi_{c1}(1P)$ and $\pi^+\psi(2S)$ invariant-mass spectra from the five data samples, together with the backgrounds from the normalized $\chi_{c1}(1P)$ or $\psi(2S)$ mass sideband events. There are no evident signals for Z_c^+ states at the expected position. No peaking backgrounds are found in the $\chi_{c1}(1P)$ or $\psi(2S)$
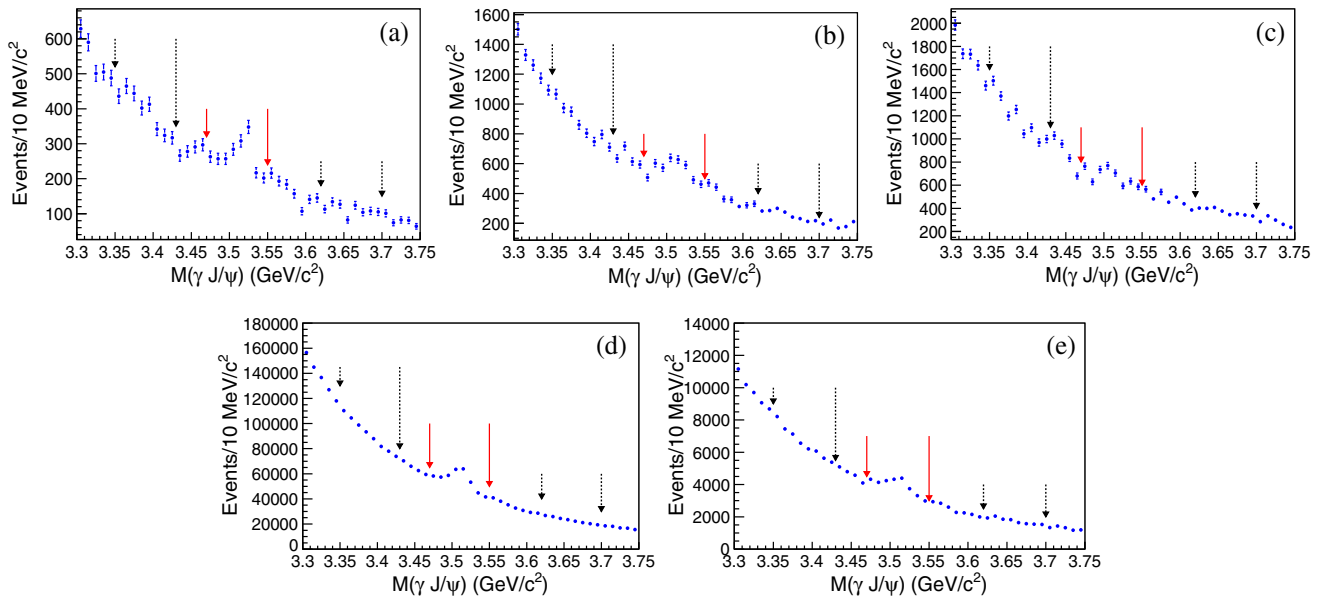
FIG. 5. The invariant-mass distributions of the $\chi_{c1}(1P)$ candidates from (a) $\Upsilon(1S)$, (b) $\Upsilon(2S)$, (c) $\sqrt{s} = 10.52$ GeV, (d) $\sqrt{s} = 10.58$ GeV, and (e) $\sqrt{s} = 10.867$ GeV data samples. The solid red arrows show the $\chi_{c1}(1P)$ signal region, and the dashed black arrows show the $\chi_{c1}(1P)$ mass sideband regions.
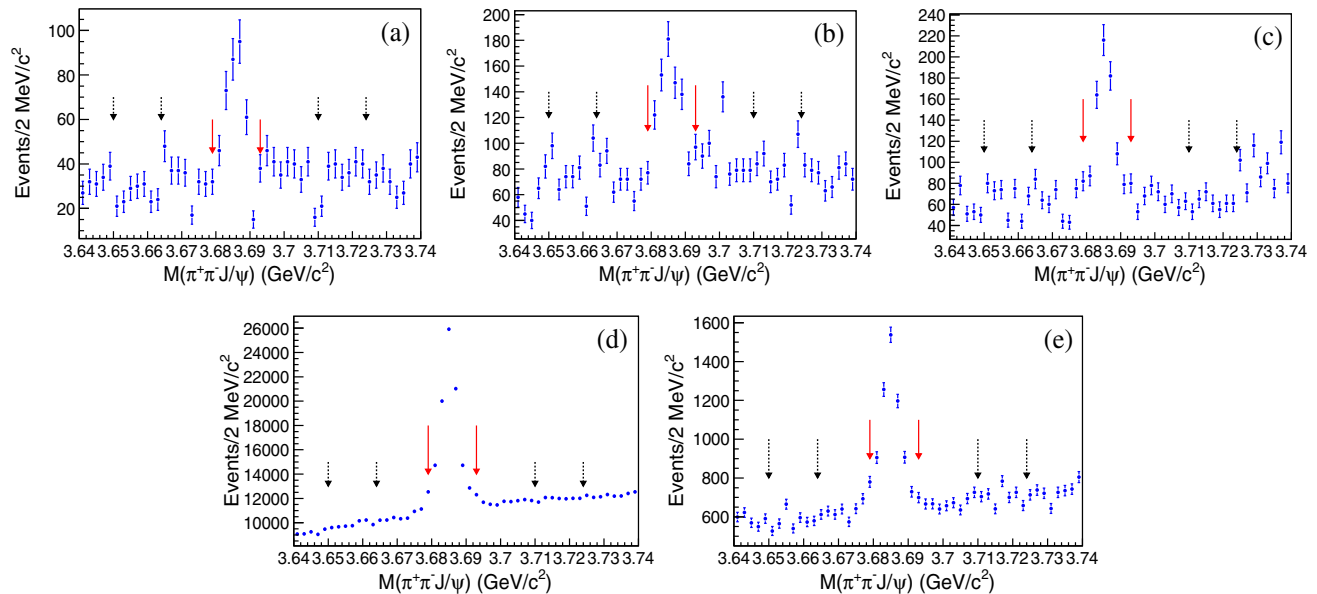

FIG. 6. The invariant-mass distributions of the $\psi(2S)$ candidates from (a) $\Upsilon(1S)$, (b) $\Upsilon(2S)$, (c) $\sqrt{s} = 10.52$ GeV, (d) $\sqrt{s} = 10.58$ GeV, and (e) $\sqrt{s} = 10.867$ GeV data samples. The solid red arrows show the $\psi(2S)$ signal region, and the dashed black arrows show the $\psi(2S)$ mass sideband regions.

mass sideband events or in the $\Upsilon(1S, 2S)$ and $e^+e^- \rightarrow q\bar{q}$ inclusive MC samples.

An unbinned extended maximum likelihood fit to the $\pi^+\chi_{c1}(1P)$ ($\pi^+\psi(2S)$) invariant-mass spectra is performed to extract the signal and background yields from $\Upsilon(1S, 2S)$ decays and $e^+e^- \rightarrow Z_c^+ Z_c^{(\prime)-}$ reactions at $\sqrt{s} = 10.52$, 10.58, and 10.867 GeV. The Z_c^+ signal probability density

functions used in the fits are the convolutions of a BW function with a Gaussian function [the parameters of BW function being fixed to the nominal masses and widths of Z_c^+ states and Gaussian functions being fixed to those from the fits to signal MC samples with mass resolutions of 15, 16, 10, and 11 MeV/c^2 for $Z_{c1}^+(4050)$, $Z_{c2}^+(4250)$, $Z_c^+(4050)$, and $Z_c^+(4250)$, respectively]. For
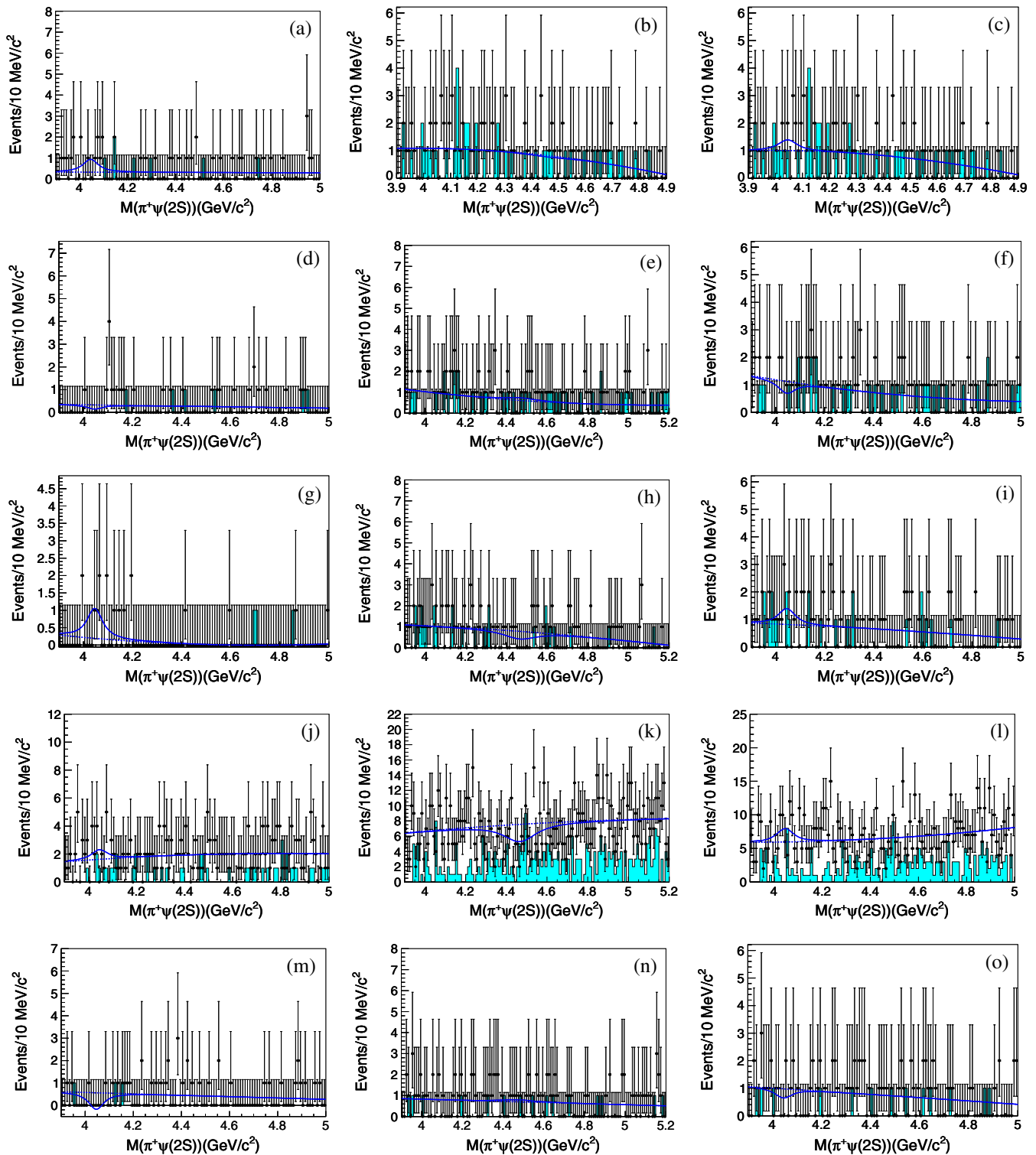
FIG. 7. The invariant-mass spectra of the Z_c^+ [$\to \pi^+ \chi_{c1}(1P)$] states in the processes (a) $\Upsilon(1S) \to Z_{c1}^+(4050)Z_{c1}^-(4050)$; (b) $\Upsilon(1S) \to Z_{c2}^+(4250)Z_{c2}^-(4250)$; (c) $\Upsilon(1S) \to Z_{c1}^+(4050)Z_{c2}^-(4250) +$ c.c.; (d) $\Upsilon(2S) \to Z_{c1}^+(4050)Z_{c1}^-(4050)$; (e) $\Upsilon(2S) \to Z_{c2}^+(4250)Z_{c2}^-(4250)$; (f) $\Upsilon(2S) \to Z_{c1}^+(4050)Z_{c2}^-(4250) +$ c.c.; (g)–(i) $e^+e^- \to Z_{c1}^+(4050)Z_{c1}^-(4050)$, $e^+e^- \to Z_{c2}^+(4250)Z_{c2}^-(4250)$, and $e^+e^- \to Z_{c1}^+(4050)Z_{c2}^-(4250) +$ c.c. at $\sqrt{s} = 10.52$ GeV; (j)–(l) $e^+e^- \to Z_{c1}^+(4050)Z_{c1}^-(4050)$, $e^+e^- \to Z_{c2}^+(4250)Z_{c2}^-(4250)$, and $e^+e^- \to Z_{c1}^+(4050)Z_{c2}^-(4250) +$ c.c. at $\sqrt{s} = 10.58$ GeV; and (m)–(o) $e^+e^- \to Z_{c1}^+(4050)Z_{c1}^-(4050)$, $e^+e^- \to Z_{c2}^+(4250)Z_{c2}^-(4250)$, and $e^+e^- \to Z_{c1}^+(4050)Z_{c2}^-(4250)$ at $\sqrt{s} = 10.867$ GeV. The solid curves are the best fits described in the text, the dotted lines are the fitted backgrounds, and the shaded histograms are from the normalized $\chi_{c1}(1P)$ mass sideband events.

FIG. 8. The invariant-mass spectra of the Z_c^+ $[\rightarrow \pi^+ \psi(2S)]$ states in the processes (a) $\Upsilon(1S) \rightarrow Z_c^+(4050)Z_c^-(4050)$; (b) $\Upsilon(1S) \rightarrow Z_c^+(4430)Z_c^-(4430)$; (c) $\Upsilon(1S) \rightarrow Z_c^+(4050)Z_c^-(4430) +$ c.c.; (d) $\Upsilon(2S) \rightarrow Z_c^+(4050)Z_c^-(4050)$; (e) $\Upsilon(2S) \rightarrow Z_c^+(4430)Z_c^-(4430)$; (f) $\Upsilon(2S) \rightarrow Z_c^+(4050)Z_c^-(4430) +$ c.c.; (g)–(i) $e^+e^- \rightarrow Z_c^+(4050)Z_c^-(4050)$, $e^+e^- \rightarrow Z_c^+(4430)Z_c^-(4430)$, and $e^+e^- \rightarrow Z_c^+(4050)Z_c^-(4430) +$ c.c. at $\sqrt{s} = 10.52$ GeV; (j)–(l) $e^+e^- \rightarrow Z_c^+(4050)Z_c^-(4050)$, $e^+e^- \rightarrow Z_c^+(4430)Z_c^-(4430)$, and $e^+e^- \rightarrow Z_c^+(4050)Z_c^-(4430) +$ c.c. at $\sqrt{s} = 10.58$ GeV; and (m)–(o) $e^+e^- \rightarrow Z_c^+(4050)Z_c^-(4050)$, $e^+e^- \rightarrow Z_c^+(4430)Z_c^-(4430)$, and $e^+e^- \rightarrow Z_c^+(4050)Z_c^-(4430) +$ c.c. at $\sqrt{s} = 10.867$ GeV. The solid curves are the best fits described in the text, the dotted lines are the fitted backgrounds, and the shaded histograms are from the normalized $\psi(2S)$ mass sideband events.

TABLE IV. Summary of the 90% C.L. upper limits on $\mathcal{B}(\Upsilon(1S, 2S) \to Z_c^+ Z_c^{(\prime)-}) \times \mathcal{B}(Z_c^+ \to \pi^+ \chi_{c1}(1P)/\pi^+ \psi(2S))$ for $Z_{c1}^+(4050)Z_{c1}^-(4050)$, $Z_{c2}^+(4250)Z_{c2}^-(4250)$, and $Z_{c1}^+(4050)Z_{c2}^-(4250) +$ c.c. to $\pi^+ \chi_{c1}(1P) +$ anything and $Z_c^+(4050)Z_c^-(4050)$, $Z_c^+(4430)Z_c^-(4430)$, and $Z_c^+(4050)Z_c^-(4430) +$ c.c. to $\pi^+ \psi(2S) +$ anything, where N^{fit} is the signal yield, N^{UL} is the 90% C.L. upper limit on the number of signal events, $\varepsilon(\%)$ is the selection efficiency, $\Sigma(\sigma)$ is the statistical signal significance, $\sigma_{\text{syst}}(\%)$ is the total systematic uncertainty, and $\mathcal{B}$ and $\mathcal{B}^{\text{UL}}$ are the branching fraction and the corresponding 90% C.L. upper limit on the branching fraction in units of 10^{-6}.

Mode	N^{fit}	N^{UL}	$\varepsilon(\%)$	$\Sigma(\sigma)$	$\sigma_{\text{syst}}(\%)$	$\mathcal{B}(\Upsilon \to Z_c^+ Z_c^{(\prime)-}) \times$ $\mathcal{B}(Z_c^+ \to \pi^+ \chi_{c1}(1P)/$ $\pi^+ \psi(2S))$	$\mathcal{B}^{\text{UL}}(\Upsilon \to Z_c^+ Z_c^{(\prime)-}) \times$ $\mathcal{B}^{\text{UL}}(Z_c^+ \to \pi^+ \chi_{c1}(1P)/$ $\pi^+ \psi(2S))$
$\Upsilon(1S) \to Z_{c1}^+(4050)Z_{c1}^-(4050)$	-2.1 ± 7.2	13.1	21.6	$\cdots$	41.3	-2.4 ± 8.1	15.8
$\Upsilon(1S) \to Z_{c2}^+(4250)Z_{c2}^-(4250)$	-8.3 ± 14.1	21.7	20.9	$\cdots$	34.5	-9.7 ± 16.8	26.6
$\Upsilon(1S) \to Z_{c1}^+(4050)Z_{c2}^-(4250) +$ c.c.	-1.3 ± 10.2	18.1	10.1	$\cdots$	25.9	-3.1 ± 24.3	44.2
$\Upsilon(2S) \to Z_{c1}^+(4050)Z_{c1}^-(4050)$	2.9 ± 7.7	16.4	20.5	0.2	38.7	2.2 ± 5.9	13.5
$\Upsilon(2S) \to Z_{c2}^+(4250)Z_{c2}^-(4250)$	8.1 ± 15.8	32.6	19.2	0.5	34.0	6.6 ± 13.2	26.7
$\Upsilon(2S) \to Z_{c1}^+(4050)Z_{c2}^-(4250) +$ c.c.	-6.3 ± 10.5	16.1	9.4	$\cdots$	18.0	-10.5 ± 17.6	27.2
$\Upsilon(1S) \to Z_c^+(4050)Z_c^-(4050)$	6.7 ± 5.3	14.4	16.0	1.4	16.4	10.0 ± 8.1	23.3
$\Upsilon(1S) \to Z_c^+(4430)Z_c^-(4430)$	-1.5 ± 7.6	13.6	16.2	$\cdots$	22.0	-2.2 ± 11.3	20.3
$\Upsilon(1S) \to Z_c^+(4050)Z_c^-(4430) +$ c.c.	4.4 ± 5.7	14.3	7.7	0.8	28.8	13.6 ± 18.1	45.5
$\Upsilon(2S) \to Z_c^+(4050)Z_c^-(4050)$	-1.9 ± 6.4	10.8	15.1	$\cdots$	16.1	-1.9 ± 6.6	11.1
$\Upsilon(2S) \to Z_c^+(4430)Z_c^-(4430)$	3.4 ± 9.6	20.0	15.3	0.3	17.8	3.4 ± 9.7	20.3
$\Upsilon(2S) \to Z_c^+(4050)Z_c^-(4430) +$ c.c.	-4.9 ± 6.2	10.2	7.5	$\cdots$	26.1	-10.1 ± 13.1	21.1

the backgrounds, a second-order Chebyshev polynomial function is adopted. The fitted results are shown in Figs. 7 and 8 and summarized in Tables IV and V.

Marginal signals are seen in each fit. The largest statistical signal significance is 2.6σ from $e^+e^- \to Z_{c2}(4250) + Z_{c2}(4250)$ at $\sqrt{s} = 10.52$ GeV. We use an ensemble of simulated experiments to estimate the probability that background fluctuations alone would produce signals as significant as those seen in the data. We generate $\pi^+ \chi_{c1}(1P)$ mass spectra based on a fitted second-order Chebyshev polynomial function alone with the same observed events in data and search for the most

TABLE V. Summary of the 90% C.L. upper limits on $\sigma(e^+e^- \to Z_c^+ Z_c^{(\prime)-}) \times \mathcal{B}(Z_c^+ \to \pi^+ \chi_{c1}(1P)/\pi^+ \psi(2S))$ for $Z_{c1}^+(4050)Z_{c1}^-(4050)$, $Z_{c2}^+(4250)Z_{c2}^-(4250)$, and $Z_{c1}^+(4050)Z_{c2}^-(4250) +$ c.c. to $\pi^+ \chi_{c1}(1P) +$ anything and $Z_c^+(4050)Z_c^-(4050)$, $Z_c^+(4430)Z_c^-(4430)$, and $Z_c^+(4050)Z_c^-(4430) +$ c.c. to $\pi^+ \psi(2S) +$ anything at $\sqrt{s} = 10.52$, 10.58, and 10.867 GeV where N^{fit} is the signal yield, N^{UL} is the 90% C.L. upper limit on the number of signal events, $\varepsilon(\%)$ is the selection efficiency, $\Sigma(\sigma)$ is the statistical signal significance, $\sigma_{\text{syst}}(\%)$ is the total systematic uncertainty, σ is the Born cross section $\sigma(e^+e^- \to Z_c^+ Z_c^{(\prime)-})$, and σ^{UL} is the corresponding 90% C.L. upper limit in units of fb.

Mode	$\sqrt{s}$ (GeV)	N^{fit}	N^{UL}	$\varepsilon(\%)$	$\Sigma(\sigma)$	$\sigma_{\text{syst}}(\%)$	$\sigma \times \mathcal{B}(Z_c^+ \to \pi^+ \chi_{c1}(1P)/ \pi^+ \psi(2S))$	$\sigma^{\text{UL}} \times \mathcal{B}(Z_c^+ \to \pi^+ \chi_{c1}(1P)/ \pi^+ \psi(2S))$
$e^+e^- \to Z_{c1}^+(4050)Z_{c1}^-(4050)$	10.52	1.2 ± 6.5	13.2	20.9	0.2	28.3	2.3 ± 12.4	25.0
$e^+e^- \to Z_{c2}^+(4250)Z_{c2}^-(4250)$	10.52	40.9 ± 16.8	65.1	19.4	2.6	32.9	83.9 ± 44.1	143.9
$e^+e^- \to Z_{c1}^+(4050)Z_{c2}^-(4250) +$ c.c.	10.52	5.2 ± 10.4	21.5	9.5	0.5	33.0	21.7 ± 44.1	93.2
$e^+e^- \to Z_{c1}^+(4050)Z_{c1}^-(4050)$	10.58	4.1 ± 18.9	36.3	20.5	0.2	21.9	1.0 ± 4.6	8.8
$e^+e^- \to Z_{c2}^+(4250)Z_{c2}^-(4250)$	10.58	-35.2 ± 48.3	25.7	19.2	$\cdots$	45.8	-9.0 ± 13.1	7.1
$e^+e^- \to Z_{c1}^+(4050)Z_{c2}^-(4250) +$ c.c.	10.58	-18.0 ± 24.8	34.5	9.8	$\cdots$	45.0	-9.1 ± 13.2	18.2
$e^+e^- \to Z_{c1}^+(4050)Z_{c1}^-(4050)$	10.867	8.6 ± 8.5	23.0	19.4	1.0	26.0	12.9 ± 13.2	35.7
$e^+e^- \to Z_{c2}^+(4250)Z_{c2}^-(4250)$	10.867	27.7 ± 16.1	49.5	18.5	1.7	27.0	43.6 ± 28.0	82.0
$e^+e^- \to Z_{c1}^+(4050)Z_{c2}^-(4250) +$ c.c.	10.867	-17.5 ± 8.6	9.4	9.1	$\cdots$	28.5	-55.7 ± 31.6	30.8
$e^+e^- \to Z_c^+(4050)Z_c^-(4050)$	10.52	9.4 ± 15.5	18.1	15.0	1.1	23.4	24.5 ± 40.8	47.7
$e^+e^- \to Z_c^+(4430)Z_c^-(4430)$	10.52	-9.7 ± 8.4	10.5	15.0	$\cdots$	16.9	-25.3 ± 22.3	29.7
$e^+e^- \to Z_c^+(4050)Z_c^-(4430) +$ c.c.	10.52	6.5 ± 7.2	18.7	7.5	0.9	17.3	33.9 ± 38.0	97.9
$e^+e^- \to Z_c^+(4050)Z_c^-(4050)$	10.58	7.7 ± 9.3	23.5	15.0	0.7	16.5	2.5 ± 3.0	7.6
$e^+e^- \to Z_c^+(4430)Z_c^-(4430)$	10.58	-60.5 ± 27.8	22.9	14.6	$\cdots$	12.7	-20.1 ± 9.6	8.3
$e^+e^- \to Z_c^+(4050)Z_c^-(4430) +$ c.c.	10.58	22.8 ± 17.2	48.5	7.3	1.3	19.5	15.1 ± 11.8	32.2
$e^+e^- \to Z_c^+(4050)Z_c^-(4050)$	10.867	-8.0 ± 3.4	5.2	14.2	$\cdots$	20.8	-16.1 ± 7.6	10.8
$e^+e^- \to Z_c^+(4430)Z_c^-(4430)$	10.867	2.7 ± 8.2	16.7	14.0	0.3	22.1	5.5 ± 16.7	35.2
$e^+e^- \to Z_c^+(4050)Z_c^-(4430) +$ c.c.	10.867	-3.7 ± 5.7	9.1	7.0	$\cdots$	21.1	-15.1 ± 23.4	39.1

TABLE VI. Relative systematic errors (%) on the measurements of the branching fractions for $\Upsilon(1S,2S) \to Z_c^+ Z_c^{(\prime)-}$ and the Born cross sections for $e^+e^- \to Z_c^+ Z_c^{(\prime)-}$ at $\sqrt{s} = 10.52$, 10.58, and 10.867 GeV, where $Z_c^+ \to \pi^+ + c\bar{c}$ $(c\bar{c}=J/\psi, \chi_{c1}(1P), \psi(2S))$.

Mode	Tracking	Particle identification	Photon	MC statistics	Branching fraction	Resonance parameter	Fit	Recoil Mass	$N_{\Upsilon(1S)/\Upsilon(2S)}$/ Luminosity	SUM
$\Upsilon(1S)/\Upsilon'(2S)/\Upsilon(2S) \to Z_c^+(3900)(\to \pi^+ J/\psi) \times Z_c^-(3900)$	1.4	3.9	⋯	1.0	1.1	10.1/5.9	20.5/13.8	9.6/6.1	2.0/2.3	25.2/16.9
$\Upsilon(1S)/\Upsilon'(2S) \to Z_c^+(4200)(\to \pi^+ J/\psi) \times Z_c^-(4200)$	1.4	3.9	⋯	1.0	1.1	18.1/22.1	9.4/10.2	18.1/19.2	2.0/2.3	27.8/31.4
$\Upsilon'(1S)/\Upsilon(2S) \to Z_c^+(3900)(\to \pi^+ J/\psi) \times Z_c^-(4200) + c.c.$	1.4	3.9	⋯	1.0	1.1	5.4/6.8	3.6/9.6	18.8/10.9	2.0/2.3	20.5/16.8
$\Upsilon(1S)/\Upsilon'(2S) \to Z_c^+(4050)(\to \pi^+ \chi_{c1}(1P))Z_{c1}^-(4050)$	1.4	3.9	2.0	1.0	3.8	15.3/6.0	35.2/36.8	14.0/8.3	2.0/2.3	41.3/38.7
$\Upsilon(1S)/\Upsilon'(2S) \to Z_c^+(4250)(\to \pi^+ \chi_{c1}(1P))Z_{c2}^-(4250)$	1.4	3.9	2.0	1.0	3.8	20.9/14.2	17.8/14.5	20.0/26.6	2.0/2.3	34.5/34.0
$\Upsilon(1S)/\Upsilon'(2S) \to Z_c^+(4050)(\to \pi^+ \chi_{c1}(1P))Z_{c2}^-(4250) + c.c.$	1.4	3.9	2.0	1.0	3.8	6.4/3.1	7.7/10.1	23.1/13.2	2.0/2.3	25.9/18.0
$\Upsilon(1S)/\Upsilon'(2S) \to Z_c^+(4050)(\to \pi^+ \psi(2S))Z_c^-(4050)$	1.8	4.6	⋯	1.0	1.5	1.9/1.3	9.6/14.8	12.0/2.5	2.0/2.3	16.5/16.1
$\Upsilon(1S)/\Upsilon'(2S) \to Z_c^+(4430)(\to \pi^+ \psi(2S))Z_c^-(4430)$	1.8	4.6	⋯	1.0	1.5	7.2/3.8	19.5/13.8	4.7/9.1	2.0/2.3	22.0/17.9
$\Upsilon(1S)/\Upsilon'(2S) \to Z_c^+(4050)(\to \pi^+ \psi(2S))Z_c^-(4430) + c.c.$	1.8	4.6	⋯	1.0	1.5	7.4/8.5	16.0/8.8	22.2/22.3	2.0/2.3	28.8/26.1
$e^+e^- \to Z_c^+(3900)(\to \pi^+ J/\psi) \times Z_c^-(3900)$ at 10.52/10.58/10.867 GeV	1.4	3.9	⋯	1.0	1.1	2.8/5.3/7.2	5.6/9.8/12.1	6.8/3.9/8.4	1.4	10.3/12.7/17.0
$e^+e^- \to Z_c^+(4200)(\to \pi^+ J/\psi)Z_c^-(4200)$ at 10.52/10.58/10.867 GeV	1.4	3.9	⋯	1.0	1.1	17.8/13.1/11.9	16.8/16.1/27.5	23.4/28.3/13.4	1.4	34.2/35.4/33.2
$e^+e^- \to Z_c^+(3900)(\to \pi^+ J/\psi)Z_c^-(4200) + c.c.$ at 10.52/10.58/10.867 GeV	1.4	3.9	⋯	1.0	1.1	5.8/7.6/5.0	1.0/1.4/4.7	21.6/18.6/14.1	1.4	22.9/20.7/16.3
$e^+e^- \to Z_c^+(4050)(\to \pi^+ \chi_{c1}(1P))Z_{c1}^-(4050)$ at 10.52/10.58/10.867 GeV	1.4	3.9	2.0	1.0	3.8	5.4/11.7/11.4	21.0/15.7/20.3	17.1/7.5/9.7	1.4	28.3/21.9/26.0
$e^+e^- \to Z_c^+(4250)(\to \pi^+ \chi_{c1}(1P))Z_{c2}^-(4250)$ at 10.52/10.58/10.867 GeV	1.4	3.9	2.0	1.0	3.8	15.7/23.1/15.4	11.8/22.4/12.5	25.6/32.0/17.3	1.4	32.9/45.8/27.0
$e^+e^- \to Z_c^+(4050)(\to \pi^+ \chi_{c1}(1P))Z_{c2}^-(4250) + c.c.$ at 10.52/10.58/10.867 GeV	1.4	3.9	2.0	1.0	3.8	9.1/7.9/10.4	21.9/32.7/12.2	22.1/29.1/22.8	1.4	33.0/45.0/28.5
$e^+e^- \to Z_c^+(4050)(\to \pi^+ \psi(2S))Z_c^-(4050)$ at 10.52/10.58/10.867 GeV	1.8	4.6	⋯	1.0	1.5	6.8/3.2/12.3	12.1/10.9/12.3	18.1/10.7/10.2	1.4	23.4/16.5/20.9
$e^+e^- \to Z_c^+(4430)(\to \pi^+ \psi(2S))Z_c^-(4430)$ at 10.52/10.58/10.867 GeV	1.8	4.6	⋯	1.0	1.5	7.2/5.3/6.1	11.7/6.5/13.3	8.4/7.9/15.6	1.4	17.0/12.8/22.1
$e^+e^- \to Z_c^+(4050)(\to \pi^+ \psi(2S))Z_c^-(4430) + c.c.$ at 10.52/10.58/10.867 GeV	1.8	4.6	⋯	1.0	1.5	4.3/8.1/5.1	7.5/9.6/9.7	14.0/13.9/17.2	1.4	17.3/19.5/21.1

significant fluctuation in each mass spectrum in the studied mass range. From these pure-background spectra, we obtain the distribution for $-2\ln(\mathcal{L}_0/\mathcal{L}_{max})$ and compare it with the signal in the data. In a total of 10,000 simulations, we find 1373 trials with a $-2\ln(\mathcal{L}_0/\mathcal{L}_{max})$ value greater than or equal to the value obtained in the data. The resulting p value is 0.1373, corresponding to a significance of 1.5σ.

Using the same method as described in the previous section, we determine the 90% C.L. upper limits on $\mathcal{B}(\Upsilon(1S,2S) \to Z_c^+ Z_c^{(\prime)-}) \times \mathcal{B}(Z_c^+ \to \pi^+ \chi_{c1}(1P)/\pi^+ \psi(2S))$ and $\sigma(e^+e^- \to Z_c^+ Z_c^{(\prime)-}) \times \mathcal{B}(Z_c^+ \to \pi^+ \chi_{c1}(1P)/\pi^+ \psi(2S))$ at $\sqrt{s} = 10.52$, 10.58, and 10.867 GeV. The values are listed in Tables IV and V, together with the signal yields (N^{fit}), the 90% C.L. upper limits on the numbers of signal events (N^{UL}), the selection efficiencies (ε), the signal significances (Σ), the systematic uncertainties (σ_{syst}) discussed below, and the central values of $\mathcal{B}(\Upsilon(1S,2S) \to Z_c^+ Z_c^{(\prime)-}) \times \mathcal{B}(Z_c^+ \to \pi^+ \chi_{c1}(1P)/\pi^+ \psi(2S))$ and $\sigma(e^+e^- \to Z_c^+ Z_c^{(\prime)-}) \times \mathcal{B}(Z_c^+ \to \pi^+ \chi_{c1}(1P)/\pi^+ \psi(2S))$, with the total errors being the sum in quadrature of the statistical and systematic errors.

VI. SYSTEMATIC ERRORS

The following sources of systematic errors are taken into account in the branching fraction and Born cross section measurements.

The systematic uncertainty due to charged-track reconstruction is determined from a study of partially reconstructed $D^{*+} \to D^0(\to K_S^0 \pi^+ \pi^-)\pi^+$ decays and is 0.35% per track. Based on the measurements of the particle identification efficiencies of lepton pairs from $\gamma\gamma \to \ell^+ \ell^-$ events and pions from a low-background sample of D^* events, the MC simulation yields uncertainties of 3.6% for each lepton pair and 1.3% for each pion. The photon reconstruction contributes 2.0% per photon, as determined from radiative Bhabha events.

The MC statistical errors are estimated using the yields of selected and generated events; these are 1.0% or less. Errors on the branching fractions of the intermediate states are taken from Ref. [23]. The uncertainties of the branching fractions for $J/\psi \to \ell^+ \ell^-$, $\chi_{c1}(1P) \to \gamma J/\psi$, and $\psi(2S) \to \pi^+ \pi^- J/\psi$ are 1.1%, 3.6% and 0.9%, respectively. The trigger efficiency, evaluated from simulation, is approximately 100% with a negligible uncertainty. We generate MC signal samples by assuming the $Z_c^+ \to \pi^+ \chi_{c1}(1P)$ decays are P-wave and find the differences between P-wave and S-wave in the selection efficiencies are less than 1% and are thus neglected.

The difference in the 90% C.L. upper limit on the signal yield when the mass and width of each $Z_c^\pm$ state are varied by 1σ is used as an estimate of the systematic uncertainty

associated with the mass and width uncertainties. By changing the order of the background polynomial and the range of the fit, the decay-mode-dependent relative difference in the 90% C.L. upper limit on signal yields is obtained and taken as the systematic error due to the uncertainty of the fit.

To estimate the systematic uncertainties due to the recoil-mass requirements for $Z_c^+ \to \pi^+ + c\bar{c}$ [$cc = J/\psi, \chi_{c1}(1P), \psi(2S)$], we optimize the recoil-mass regions again by changing the Z_c^+ widths by 1σ and take the differences in the 90% C.L. upper limits on the signal yields as systematic uncertainties.

Changing the s dependence of the cross sections of $e^+e^- \to Z_c^+ + Z_c^{(\prime)-}$ from $1/s^2$ to $1/s^6$, the radiative correction factors $(1 + \delta)_{\mathrm{ISR}}$ become 0.651, 0.659, and 0.655 for $\sqrt{s} = 10.52$, 10.58, and 10.867 GeV, respectively. The differences are less than 1% and are thus neglected.

The uncertainties on the total numbers of $\Upsilon(1S)$ and $\Upsilon(2S)$ events are 2.0% and 2.3%, respectively, which are mainly due to imperfect simulations of the charged-track multiplicity distributions from inclusive hadronic MC events. Finally, the total luminosity is determined to 1.4% precision using wide-angle Bhabha scattering events.

All the systematic uncertainties are summarized in Table VI for the measurements of $\Upsilon(1S,2S) \to Z_c^+ Z_c^{(\prime)-}$ and $e^+e^- \to Z_c^+ Z_c^{(\prime)-}$ at $\sqrt{s} = 10.52$, 10.58, 10.867 GeV, where $Z_c^+ \to \pi^+ + c\bar{c}$ ($c\bar{c} = J/\psi, \chi_{c1}(1P), \psi(2S)$). Assuming all the sources are independent and adding them in quadrature, the total systematic uncertainties are obtained for each mode.

VII. CONCLUSION

In summary, using the large data samples of 102×10^6 $\Upsilon(1S)$ events; 158×10^6 $\Upsilon(2S)$ events; and 89.5 fb^{-1}, 702.6 fb^{-1}, and 121.1 fb^{-1} at $\sqrt{s} = 10.52$, 10.58, and 10.867 GeV, respectively, collected by Belle, we search for $\Upsilon(1S,2S) \to Z_c^+ Z_c^{(\prime)-}$ and $e^+e^- \to Z_c^+ Z_c^{(\prime)-}$ at $\sqrt{s} = 10.52$, 10.58, and 10.867 GeV with $Z_c^+ \to \pi^+ + c\bar{c}$ [$c\bar{c} = J/\psi, \chi_{c1}(1P), \psi(2S)$]. No clear signals are observed in the studied modes. We determine the 90% C.L. upper limits on $\mathcal{B}(\Upsilon(1S,2S) \to Z_c^+ Z_c^{(\prime)-}) \times \mathcal{B}(Z_c^+ \to \pi^+ + c\bar{c})$ and $\sigma(e^+e^- \to Z_c^+ Z_c^{(\prime)-}) \times \mathcal{B}(Z_c^+ \to \pi^+ + c\bar{c})$ at $\sqrt{s} = 10.52$, 10.58, and 10.867 GeV. The results are displayed graphically in Figs. 9 and 10. Due to G-parity conservation, our studied processes are electromagnetic, i.e., can only proceed through a virtual photon, which then transforms into a light-quark pair ($u\bar{u}$) or ($d\bar{d}$). In this case, the dynamical suppression is much larger due to the production of two ($c\bar{c}$) pairs. The expected production cross section should be much lower than the double charmonium processes like $e^+e^- \to J/\psi\eta_c$ [30]. The reported upper limits are not in contradiction with the naive expectation.

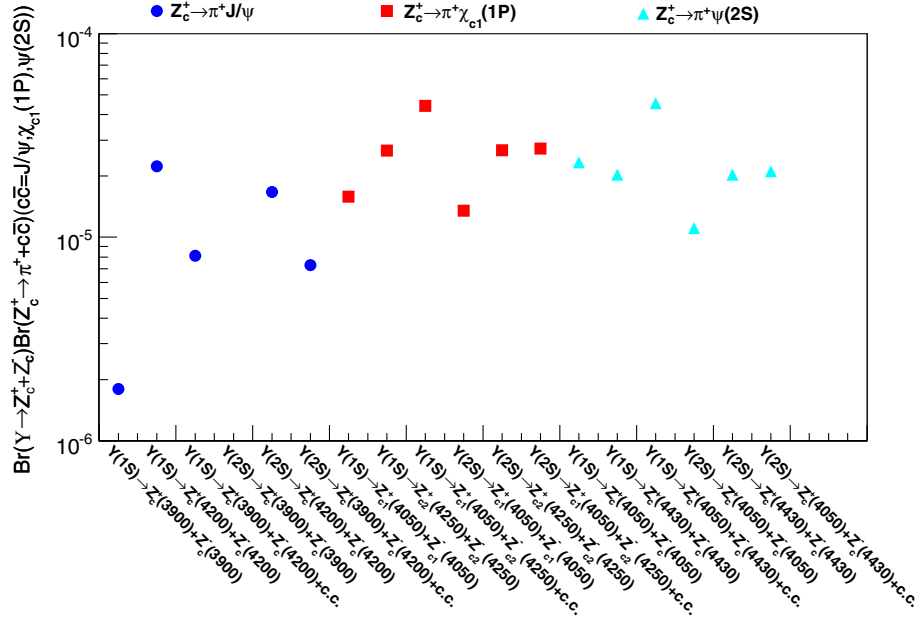FIG. 9. The 90% C.L. upper limits on $\mathcal{B}(\Upsilon(1S, 2S) \to Z_c^+ Z_c^{(\prime)-}) \times \mathcal{B}(Z_c^+ \to \pi^+ + c\bar{c})$ [$c\bar{c} = J/\psi, \chi_{c1}(1P), \psi(2S)$]. The blue circles represent the results for modes $Z_c^+ \to \pi^+ + J/\psi$, red boxes represent the results for $Z_c^+ \to \pi^+ + \chi_{c1}(1P)$, and cyan triangles represent results for $Z_c^+ \to \pi^+ + \psi(2S)$.
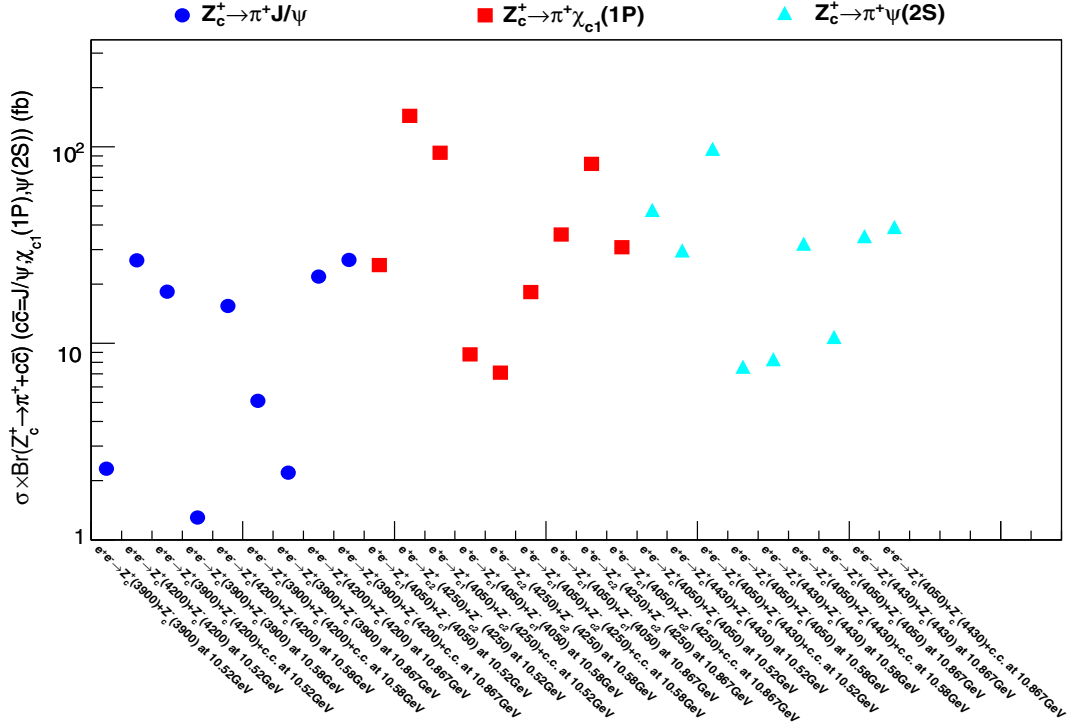

FIG. 10. The 90% C.L. upper limits on $\sigma(e^+ e^- \to Z_c^+ Z_c^{(\prime)-}) \times \mathcal{B}(Z_c^+ \to \pi^+ + c\bar{c})$ [$c\bar{c} = J/\psi, \chi_{c1}(1P), \psi(2S)$] at $\sqrt{s} = 10.52, 10.58,$ and 10.867 GeV. The blue circles represent the results for modes $Z_c^+ \to \pi^+ + J/\psi$, red boxes represent results for $Z_c^+ \to \pi^+ + \chi_{c1}(1P)$, and cyan triangles represent results for $Z_c^+ \to \pi^+ + \psi(2S)$.

ACKNOWLEDGMENTS

[1] For a recent review, see H. X. Chen, W. Chen, X. Liu, and S. L. Zhu, Phys. Rep. **639**, 1 (2016).

[2] S. K. Choi *et al.* (Belle Collaboration), Phys. Rev. Lett. **100**, 142001 (2008).

[3] R. Mizuk *et al.* (Belle Collaboration), Phys. Rev. D **78**, 072004 (2008).

[4] M. Ablikim *et al.* (BESIII Collaboration), Phys. Rev. Lett. **110**, 252001 (2013).

[5] Z. Liu *et al.* (Belle Collaboration), Phys. Rev. Lett. **110**, 252002 (2013).

[6] K. Chilikin *et al.* (Belle Collaboration), Phys. Rev. D **90**, 112009 (2014).

[7] X. L. Wang *et al.* (Belle Collaboration), Phys. Rev. D **91**, 112007 (2015).

[8] R. Aaij *et al.* (LHCb Collaboration), Phys. Rev. Lett. **112**, 222002 (2014).

[9] M. Ablikim *et al.* (BESIII Collaboration), Phys. Rev. Lett. **119**, 072001 (2017).

[10] S. L. Olsen, T. Skwarnicki, and D. Zieminska, Rev. Mod. Phys. **90**, 015003 (2018).

[11] N. Brambilla *et al.*, Eur. Phys. J. C **71**, 1534 (2011).

[12] N. Brambilla *et al.*, Eur. Phys. J. C **74**, 2981 (2014).

[13] C. Z. Yuan, Int. J. Mod. Phys. A **29**, 1430046 (2014).

[14] S. J. Brodsky, R. F. Lebed, and V. E. Lyubovitskij, Phys. Lett. B **764**, 174 (2017).

[15] S. J. Brodsky and R. F. Lebed, Phys. Rev. D **91**, 114025 (2015).

[16] Throughout this analysis, for any given mode, the corresponding charge-conjugate mode is implied.

[17] A. Abashian *et al.* (Belle Collaboration), Nucl. Instrum. Methods Phys. Res., Sect. A **479**, 117 (2002).

[18] S. Kurokawa and E. Kikutani, Nucl. Instrum Methods Phys. Res., Sect. A **499**, 1 (2003) and other papers included in this volume.

[19] J. Brodzicka *et al.*, Prog. Theor. Exp. Phys. **2012**, 04D001 (2012).

[20] D. J. Lange, Nucl. Instrum. Methods Phys. Res., Sect. A **462**, 152 (2001).

[21] Y. Tosa, Report No. DPNU-34-1976, http://inspirehep.net/record/109354?ln=zh_CN.

[22] T. Sjöstrand, S. Mrenna, and P. Skands, J. High Energy Phys. 05 (2006) 026.

[23] C. Patrignani *et al.* (Particle Data Group Collaboration), Chin. Phys. C **40**, 100001 (2016) and 2017 update.

[24] E. Nakano, Nucl. Instrum. Methods Phys. Res., Sect. A **494**, 402 (2002).

[25] K. Hanagaki, H. Kakuno, H. Ikeda, T. Iijima, and T. Tsukamoto, Nucl. Instrum. Methods Phys. Res., Sect. A **485**, 490 (2002).

[26] A. Abashian *et al.*, Nucl. Instrum. Methods Phys. Res., Sect. A **491**, 69 (2002).

[27] E. A. Kuraev and V. S. Fadin, Yad. Fiz. **41**, 733 (1985) [Sov. J. Nucl. Phys. **41**, 466 (1985)].

[28] S. Actis *et al.*, Eur. Phys. J. C **66**, 585 (2010).

[29] In common high-energy physics usage, this Bayesian interval has been reported as the "confidence interval," which is a frequentist-statistics term.

[30] K. Abe *et al.* (Belle Collaboration), Phys. Rev. D **70**, 071102 (2004).